Science of the Total Environment 976 (2025) 179299

Contents lists available at ScienceDirect

Science of the Total Environment

journal homepage: www.elsevier.com/locate/scitotenv

Modelling the hydrological response of blue-green roofs: ECO-PRO model

Dario Pumo *, Matteo Ippolito, Francesco Alongi, Antonio Francipane, Leonardo V. Noto

Dipartimento di Ingegneria - Università degli Studi di Palermo, Viale delle Scienze, Ed. 8, 90128 Palermo, Italy

HIGHLIGHTS

- ECO-PRO simulates the hydrologic response of Multi-layer Green Roofs (MGRs).
- Three years of rainfall, soil moisture & runoff data at case study were used for its development.
- R^2 was 0.88 for daily runoff & 0.91 for event-scale stormwater retention rates.
- ECO-PRO showed low sensitivity to parameters and epistemic uncertainty.
- Soil parameters had the greatest influence on model outputs.

GRAPHICAL ABSTRACT

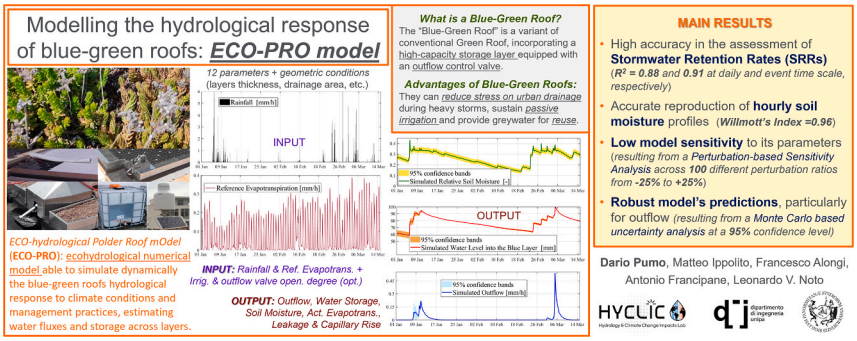

ARTICLE INFO

Editor: Wei Ouyang

Keywords:
Urban stormwater management
Climate change
Ecohydrology
Retention
Nature based solution
Urban floods mitigation
Climate adaptive solution

ABSTRACT

Green roofs are climate-adaptive measures able to address many urban challenges like heat islands, water scarcity, floodings, pollution and biodiversity loss. Recently, the "blue-green roof" variant has gained attention for its enhanced functionality, since, incorporating a high-capacity storage layer, they can retain significant amount of rainwater. This last can be gradually released, reducing stress on urban drainage during heavy storms, sustain passive irrigation and provide greywater for reuse. Modelling green infrastructures is essential for optimizing design and efficacy, and, in this context, ecohydrological models, which capture the complex ecological and hydrological interactions, offer a valuable option.

This study introduces the ECO-hydrological Polder Roof mOdel (ECO-PRO), a tailored ecohydrological model specifically for multilayer green roofs. ECO-PRO is a numerical model able to simulate dynamically the blue-green roofs hydrological response to climate conditions and management practices, estimating water flow and storage across layers. The model was implemented based on an experimental site in Palermo (Italy), using a high-resolution dataset and performing parameters optimization through genetic algorithms. Simulated water fluxes and time series of soil moisture and outflow generated by the system demonstrated strong alignment with observed data over a three-year monitoring period, with robust performance indicators. Notably, the coefficient of determination (R^2) for daily runoff was 0.88. Parameter sensitivity and uncertainty assessments further validated the model's reliability. A test model application accurately captured stormwater retention after prolonged rainy spells (R^2 = 0.91), confirming its effectiveness for the dynamic assessment of water volumes released and retained by the system.

* Corresponding author.
E-mail addresses: dario.pumo@unipa.it (D. Pumo), matteo.ippolito@unipa.it (M. Ippolito), francesco.alongi01@unipa.it (F. Alongi), antonio.francipane@unipa.it (A. Francipane), leonardo.noto@unipa.it (L.V. Noto).

https://doi.org/10.1016/j.scitotenv.2025.179299
Received 10 January 2025; Received in revised form 28 March 2025; Accepted 28 March 2025
Available online 9 April 2025

1. Introduction

Cities exert significant ecological pressures, consuming most natural resources and generating approximatively 75 % of global carbon emissions (Fragkias et al., 2013). Climate change intensifies these pressures, by increasing frequency and magnitude of heatwaves, extreme rainfall, and water scarcity, particularly impacting the Mediterranean (IPCC, 2021; Noto et al., 2023; von Schuckmann et al., 2023). Rapid population growth and urbanization (UN, 2019), further heighten resource demand in cities and favour the replacement of natural surfaces with impervious materials. This exacerbates urban runoff, often overloading drainage systems and leading to floods. Traditional urban drainage systems are designed according to a "resistance paradigm" and under the "static" probabilistic principle of the "return period", which relies on historical climate patterns. Consequently, these systems are unable to adapt effectively to evolving stormwater dynamics in rapidly expanding cities. These emerging urban challenges, along with the increasing biodiversity loss, pose significant risks to infrastructures and human health, incurring high social costs (Santamouris, 2020; Pörtner et al., 2023).

Nature-Based Solutions (NBSs) offer adaptive approaches to such challenges (Faivre et al., 2017), aligning with Sustainable Development Goals (UN, 2015) and policies like the European Green Deal and Next-GenerationEU. Many NBSs promote small-scale hydrologic control for stormwater infiltrating, filtering, evaporating, and detaining at the source (Ercolani et al., 2018), fostering hydrologic-hydraulic invariance (Raymond et al., 2017; Seddon et al., 2021). Green Roofs (GRs) are particularly promising NBSs for urban environments (Cook and Larsen, 2020), since they support urban regeneration, improve building energy efficiency, reduce Urban Heat Island (UHI) effects (Getter et al., 2011; Ávila-Hernández et al., 2023), decrease noise and air pollution (Yang et al., 2008), and enhance biodiversity. Specific GR configurations can help mitigate stormwater challenges and improve water quality (Ercolani et al., 2018; Suszanowicz and Kolasa Więcek, 2019). GRs also offer social advantages, such as recreational spaces and urban agriculture opportunities, which benefit public health (Vijayaraghavan, 2016; Jenkins, 2020).

Multilayer Green Roofs (MGRs), featuring a high-capacity water storage layer (Blue Layer, BL), combine the advantages of traditional GRs with Rainwater Harvesting Systems (RHSs) capabilities, so that MGRs are often considered as hybrid solutions, named "blue-green roofs" (Brears, 2018; Almeida et al., 2023). A MGR may be a versatile solution to adapt to extreme weather fluctuations predicted under climate change (Shafique et al., 2016; Andenæs et al., 2018), and are well-suited for arid or semi-arid regions, where conventional GRs may encounter difficulties due to prolonged dry conditions. The BL facilitates passive irrigation (Cirkel et al., 2018), mitigating potential water stress, and allows rainwater reuse.

However, specific studies on MGRs are still limited and their numerous benefits remain largely unquantified. The systematic monitoring and the development of reliable models to assess GRs and MGRs under various climate scenarios are essential for integrating these technologies into sustainable urban planning and shaping incentivizing strategies (Versini et al., 2015; Johannessen et al., 2019). In particular, for MGRs, understanding water distribution dynamics within the system is crucial for optimizing design and management oriented to predefined objectives, like water reuse and flood mitigation.

Many modelling tools have been used to simulate conventional GRs, from empirical relations (Liu et al., 2019) to event-based hydrological models (Lamera et al., 2014) and conceptual models (Carbone et al., 2014). Some thermal simulation software (e.g., EnergyPlus DT, 2019), can be used for a rough estimation of the hydrological performance of GRs based on extremely simplified water balance equations. However, numerical approaches based on stormwater-specific software, such as SWMM (Rossman, 2015), MIKE URBAN (DHI, 2017), and HYDRUS (Feitosa and Wilkinson, 2016), are generally preferred for modelling hydrological aspects of GRs (Locatelli et al., 2014; Peng and Stovin, 2017). Nevertheless, most of these models rely on empirical parameters with limited validation from field data, primarily due to scarce monitoring. It is also often argued that such models are too computationally expensive to be integrated in decision support tools (Soulis et al., 2017), since they require accurate physical parameters and specific substrate information that can be difficult to obtain or measure (Hakimdavar et al., 2016) and that can highly affect results (Hernes et al., 2020). Specific applications of such software for MGRs are almost completely absent. The inclusion of a high-capacity water storage layer, hydraulically connected to the vegetated layer and equipped with an outflow control valve, makes hydrological modelling for MGR more complex than for conventional GRs, necessitating dedicated models to accurately simulate stormwater attenuation, rainwater storage, and reuse capacities under variable conditions (Yan et al., 2024).

This study presents a new ecohydrological model for MGRs, named ECO-PRO (ECO-hydrological Polder Roof mOdel). The model is lumped and based on the numerical resolution of two coupled water balance equations: one for the vegetation-soil layer (Green Layer, GL) and another for the buffer layer (BL). The model is forced by hourly rainfall and reference evapotranspiration and can incorporate dynamic management rules by inputting time series of irrigation and closure degrees of the outflow control valve. As outputs, the model provides hourly time series of canopy interception, evapotranspiration, leakage and capillary rise water fluxes, soil moisture, water levels within the BL and outflow generated by the system.

ECO-PRO is designed to be parsimonious, with only 12 parameters. It was developed based on a technologically advanced experimental site in Palermo (Italy), highly monitored since 2020 by a complex network of sensors (Pumo et al., 2023a,b). Measured rainfall, irrigation water volumes, soil moisture and outflow were used for model calibration and validation alongside reference evapotranspiration derived using reanalysis data. Calibration spanned over two years, with a third year used exclusively for validation. Parameters optimization around knowledge-based values was performed using genetic algorithms. Model performances, evaluated through various metrics, showed a high matching degree between observed and simulated traces of soil moisture and outflow. A further application has demonstrated ECO-PRO's suitability and versatility for different practical purposes. ECO-PRO, with opportune adaptations, could be used across different settings and climate scenarios, and offers a valuable decision-support tool for green infrastructure investments and implementations in urban areas.

The paper is structured as follows. Section 2 introduces case study and model, detailing procedures used for calibration, sensitivity, and uncertainty analyses. Model performances and the results of sensitivity and uncertainty analyses are described in Section 3, along with the demonstrative application. This last was specifically designed to assess the potential contribution of the MGR in terms of stormwater retention after significantly wet periods and evaluate the role of the different layers in the retention function of the system. Section 4 discusses results, followed by concluding remarks.

2. Materials and methods

2.1. The Polder Roof of Palermo and its monitoring system

The experimental site (Fig. 1) is an advanced prototype, named Polder Roof, developed by the Metro-Polder company and installed on a rooftop at the University of Palermo (Italy) in 2019 as part of the project *Polder Roof Field Lab*, supported by the EIT Climate-KIC program (Cristiano et al., 2022).

Palermo's climate, classified as *Csa* (*Hot-summer subtropical Mediterranean climate*), under the Köppen-Geiger system, is marked by hot and dry summers and rainy winters. Data from 2002 to 2022, recorded at gauge station Uditore of the SIAS (*Servizio Informativo Agrometeorologico Siciliano*) regional agency, located approximately 3 km from the site, show mean annual air temperature of 18.9 °C, and mean

annual precipitation of 740 mm, with approximately 75 % occurring in autumn and winter.

The Polder Roof follows the concept of Multilayer-Green Roofs (MGRs), comprising a high-capacity blue layer (BL) beneath a green layer (GL). Rainfall not intercepted by the vegetation infiltrates through the GL, increasing soil moisture. Once soil's field capacity is exceeded, excess water percolates into the BL where it is retained until the storage retention capacity, regulated dynamically by the outflow weir, is reached. The BL, thus, provides storage for reuse in non-potable applications, such as greywater supply and passive irrigation through capillary cones, connecting the BL with the GL. When the percolation exceeds the BL retention capacity, surplus water is discharged from the system as outflow. The general functioning of the MGR and its enhanced effect of lamination are explained in detail in Pumo et al. (2023a).

The MGR covers 32.1 m^2 divided into two zones with different soil depths: a central 18.0 m^2 area with 20 cm depth, and a 14.1 m^2 border region with 10 cm depth. The substrate consists of a mixture of volcanic lapillus (90 %) and pumice (10 %), conforming to the Italian standard UNI 11235 (2015). This fertile soil provides high drainage, hydraulic conductivity and water retention, which, along with lateral aluminium barriers surrounding the GL, prevent from the generation of surface runoff for saturation excess even during intense storms. Vegetation includes a selection of Mediterranean vegetation and *crassulaceae* plants, with a prevalence of typical autochthonous species for Sicily, rather drought-tolerant once established. Various sedum and typical meadow species (e.g., *sedum album*, *sedum sediforme*, *stipa capensis*, *trifolium angustifolium*, *aegylops geniculata* and *silene coeli-rosa*) cover the shallower sub-region, while the deeper area is prevalently covered by aromatic species (e.g., *rosmarinus officinalis*, *teucrium fruticans*, *lavandula spica*, *coridothymus capitatus*, *origanum heracleoticum*). Some seasonal spontaneous species (e.g., *oxalis pes-caprae*) are periodically removed after their life cycle to maintain a balanced ecosystem. Therefore, the overall vegetation system can be seen as a complex dynamic green system evolving in time in response to seasonal and climatic changes and the maintenance practices applied (Schrieke et al., 2023).

The BL, separated from the GL by a capillary geotextile drainage membrane, is 10 cm deep and can store nearly 2500 l of water. It includes a modular system with plastic support units and capillary cones (*Permavoid system*), a protective geotextile filter fabric, and a waterproof membrane. The BL is equipped with a remote-controlled semi-automatic outflow control weir, clearly visible in the left picture of Fig. 1, which was however constantly set at its maximum closure degree ($c_{dg} = 1$), corresponding to a weir height of 8 cm.

Manual irrigation, measured by a flowmeter, was supplied during dry periods until July 2023, when an automatic irrigation system, with 120 drippers and an automatic controller (Gardena Water Control Flex), was installed to improve water distribution and control. The site has been monitored since Dec. 2020 by a Polder Roof integrated monitoring system, SmˆrtMILL, which tracks variables like precipitation, air temperature, and wind speed in real-time. Data, acquired with frequency of 10 min, are transmitted to an online dashboard, AQORA, by which it is also possible to regulate the control weir. The integrated equipment also included a sensor of BL water levels neglected in this study; this sensor was, in fact, working only for a limited period (from Jan. 13rd to Jun. 29th, 2021), and numerous anomalies and data inconsistencies rendered the readings unsuitable for analysis.

An adjacent weather monitoring station 65 m far from the site, described in detail in Lo Conti et al. (2015), provides high resolution meteorological data, which are freely accessible at the HYCLIC (*HYdrology & Climate change ImpaCts Lab*) website (http://idrologia.unipa.it/). This station is equipped with three different sensors of rainfall with 1-min acquisition frequency: a weighing rain gauge (OTT Pluvio2-400), a laser-optic disdrometer (OTT- Parsivel2) and a tipping bucket rain gauge (LSI LASTEM - DQA130.1). It also includes a thermo-hygrometer, and an air pressure sensor not considered in this study. Outflow from the BL is directed to a 1000 l external rain barrel and continuously measured (acquisition frequency of 5 min) using a couple of pressure sensors (i.e., vanEssen micro-diver and baro-diver barometric pressure loggers).

A set of thermometers also track indoor and outdoor roof temperatures every 30 min. Recent enhancements to the monitoring system include the following additional sensors operative from Feb, 2024: a 3D sonic anemometer, a net radiometer, a thermos-hygrometer probe, a self-calibrating heat flux plate, six averaging soil thermocouple probes, and five water content reflectometers, WCR (CS616 by Campbell Scientific), buried at different positions across the GL and gathering data at 15-min intervals. Additionally, since Dec. 2023, periodic field campaigns have also been conducted to sample spot soil water content at 14 fixed points, homogeneously distributed across the GL, using a portable soil moisture meter (TDR 6440FS, Spectrum Technologies Inc.) with probes of 3.8 cm for the shallower area (8 points) and 12 cm for the deeper region (6 points).

Fig. 1. Pictures of the experimental site taken on different days in 2023. The left picture highlights the SmˆrtMILL system and the outflow control weir.

2.2. Description of the model

The ECO-hydrological Polder Roof mOdel (ECO-PRO) is a lumped model for MGRs which simulates the temporal dynamics of soil moisture (s), and BL water levels (h), and outflow (OUT) by integrating climatic, pedological, and vegetational attributes. Its hydrological conceptualization, depicted in Fig. 2, comprises a two-bucket element, associated with the GL, and a reservoir with an outflow weir, associated to the BL.

The fundamental principle guiding the model's development was simplicity, wherein the reduction of parameters was prioritized in the attempt to concentrate uncertainties arising from data and model structure. The model is based on the numerical solution, at the hourly time-scale, of the following system of two water balance equations:

$$\begin{cases} \Delta s = s_{i+1} - s_i = \left(\frac{\varphi_i}{n \cdot Z_r} - \frac{\chi_i}{n \cdot Z_r}\right) \cdot \Delta t \\ \Delta h = h_{i+1} - h_i = L_i(s_i) + R_i\left(s_i, I_{rr,i}, P_i, I_i\right) - U_{s,i}(s_i, PET_i, h_i) - E_{b,i}(PET_i h_i) - OUT(h_i) \end{cases} \quad (1)$$

The former water balance equation pertains to the GL, while the latter to the BL. The various terms of Eq. (1) are explained and discussed individually in the following sections.

2.2.1. Water balance equation for the Green Layer

Adopting a classical ecohydrological approach (Rodriguez-Iturbe and Porporato, 2004), the soil-vegetation system is assumed homogeneous in soil and plant properties, with depth equal to the average depth

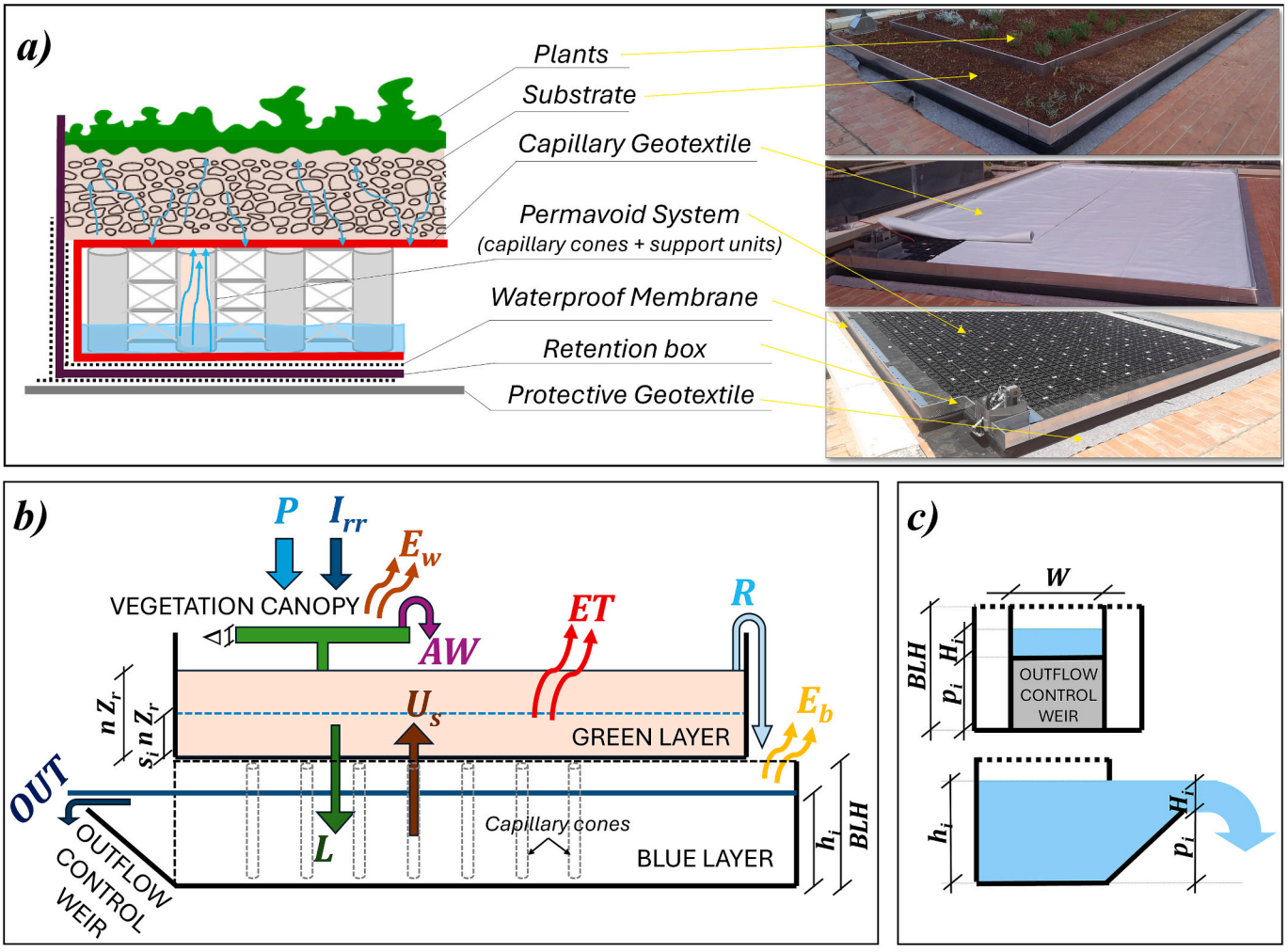

Fig. 2. Schematic conceptualization of the MGR (symbols are explained in Sections 2.2). a) Cross-sectional view of the system, including a detailed characterization of its structure, and inset figures displaying photos highlighting specific components of the system. b) The vegetation canopy and the Green Layer (GL) are conceptualized by bucket elements with capacity Δ and $n \cdot Z_r$, respectively; $s_i \cdot n \cdot Z_r$ (mm) is the water storage into the GL at the generic time i, with relative soil moisture s_i. The Blue Layer (BL) is conceptualized as a reservoir with height BLH and an inclined rectangular weir with regulable opening degree (c_{dg}). Capillary cones connect the BL with the GL. The BL water level at the generic time i is denoted as h_i (mm). The hydrological components of the water balance at each layer are also depicted using different colors. c) Schematic representations of the outflow weir, in front (upper scheme) and side (bottom scheme) view. The weir has length W and variable height p_i, which determinates the maximum retention capacity of the BL, while H_i is the head over the weir.

of the GL, and root zone interesting the full GL thickness.

Both soil and vegetation characteristics are assumed time-invariant, disregarding surface effects induced by raindrop impact (e.g., soil crusting, sealing, etc.), as well as potential long-term changes, such as the increase in soil organic matter content over time (Getter et al., 2007; Spolek, 2008). Additionally, seasonal variations in vegetation coverage are not considered (i.e. assuming a stationary "mean" vegetation, with an "average behaviour"). A horizontally and vertically averaged relative soil water content, s, is used in Eq. (1) to represent water within the GL. This assumption is based on the negligible lateral water movement on flat roofs and rapid redistribution of moisture within the root zone due to the plants capacity to compensate for spatial variations in saturation (Guswa et al., 2002).

The GL water balance equation, reported in the first relationship of Eq. (1) and solved through a finite difference method (Pumo et al., 2008; Viola et al., 2014), calculates soil moisture variation (Δs) in the GL on an hourly time-step ($\Delta t = 1$ h). The subscripts i and $i + 1$ in Eq. (1) refer to the beginning and the ending of the time-step. The terms n and Z_r are the soil porosity and the root depth (equal to the mean depth of the GL), respectively.

The term φ_i denotes the water flux incoming into the GL at time t_i and it is given by:

$$\varphi_i = I_{rr,i} + P_i - I_i\left(I_{rr,i}, P_i, E_{w,i}\right) - R_i\left(s_i, I_{rr,i}, P_i, I_i\right) + U_{s,i}(s_i, PET_i, h_i) \tag{2}$$

where $I_{rr,i}$ is the irrigation water depth, P_i is the rainfall, $U_{s,i}$ is the capillary rise flux from the BL, while I_i and R_i are the aliquots of incoming water not infiltrating and lost via canopy interception and surface runoff, respectively.

Interception (I_i), is modelled with a bucket approach, where a fixed threshold (Δ) represents the maximum canopy water storage. This, according to Rodriguez-Iturbe and Porporato (2004), can vary from few millimetres for grass to few centimetres for trees. The interception module in ECO-PRO computes dynamically an interception storage capacity (c_i) at given time t_i, ranging from zero, when canopy is no longer able to intercept water due to previously intercepted rainfall, to Δ, reached after long dry periods. When incoming water ($I_{rr,i} + P_i$) does not exceed c_i, it is entirely retained by the plants ($I_i = I_{rr,i} + P_i$), no water reaches the ground and c_i reduces consequentially (i.e., $c_{i+1} = c_i - I_i$). On the contrary, when incoming water exceeds c_i, the surplus (i.e., $I_{rr,i} + P_i - c_i$) infiltrates into the soil, the interception terms I_i is equal to c_i, and the interception capacity at the following step become null ($c_{i+1} = 0$). During dry steps ($I_{rr,i} + P_i = 0$), I_i is null and the interception capacity replenishes via direct evaporation ($E_{w,i}$), increasing (i.e., $c_{i+1} = c_i + E_{w,i}$) up to the threshold Δ.

Surface runoff (R_i) follows a Dunnian saturation mechanism and occurs only when water arriving at the soil surface ($AW_i = P_i + I_{irr} - I_i$) exceeds its instantaneous storage capacity, SSC_i, given by $(1\text{-}s_i)\cdot n\cdot Z_r$. The term R_i is given by the surplus (AW_i - SSC_i) and is instantaneously routed to the BL. However, given the GL high hydraulic conductivity, runoff is rare and was not observed during the study period.

The capillary rise flux, $U_{s,i}$, simulates the processes of exfiltration, which allows water from the BL to reach the GL through capillary cones. It can occur only when leakage is absent and it is simulated by a specific module of the *wflow_sbv model* (Seizarwati and Syahidah, 2021), included in the open source *wflow* platform (Deltares, 2016). This model, derived from the *topog_sbm model* (Vertessy and Elsenbeer, 1999), calculates capillary rise as the product of a potential capillary rise term (PCR_i) and a scaling factor CSF_i, as:

$$\begin{cases} U_{s,i} = PCR_i \cdot CSF_i \\ PCR_i = min[(k_{sat}\cdot\Delta t); (ET_i\cdot\Delta t); (1 - s_i)\cdot n\cdot Z_r\,; h_i] \\ CSF_i = \dfrac{CS}{CS + BLH - h_i} \end{cases} \tag{3}$$

PCR_i is the maximum possible capillary rise in a time step Δt, constrained by the saturated soil conductivity (k_{sat}), the actual evapotranspiration (ET_i), the soil moisture deficit with respect to saturation, $(1\text{-}s_i)\cdot n\cdot Z_r$, and the water level in the BL (h_i). The scaling factor CSF_i reduces PCS_i in proportion to the distance between the root depth and water surface in the BL ($BLH\text{-}h_i$). BLH is the thickness of the BL, which, under the assumptions made for ECO-PRO, is also corresponding to the distance of the root zone from the BL bottom surface, while CS is a parameter.

The term χ_i in Eq. (1) denotes water losses from the GL at the generic time t_i due to the evapotranspiration (ET_i) and the leakage (L_i), and it is computed as:

$$\chi_i = ET_i(s_i, PET_i) + L_i(s_i) \tag{4}$$

with the evapotranspiration and leakage terms respectively given by:

$$ET_i = \begin{cases} E_{w,i}\cdot\dfrac{s_i - s_h}{s_w - s_h} & for\ s_h \le s_i < s_w \\ E_{w,i} + \left(PET_i - E_{w,i}\right)\dfrac{s_i - s_w}{s^* - s_w} & for\ s_w \le s_i < s^* \\ PET_i & for\ s^* \le s_i \le 1 \end{cases} \tag{5}$$

$$L_i = \begin{cases} 0 & for\ s_i \le s_{fc} \\ k_{sat}\cdot\dfrac{\left[e^{\beta\cdot\left(s_i - s_{fc}\right)} - 1\right]}{\left[e^{\beta\cdot\left(1 - s_{fc}\right)} - 1\right]} & for\ s_{fc} < s_i \le 1 \end{cases} \tag{6}$$

Water loss through actual evapotranspiration (ET) and leakage (L_i), depends on relative soil moisture (s), calculated with a stepwise function. When s is below the wilting point, s_w, plants cannot uptake water, so only direct evaporation occurs; this is conceptualized considering a linear function ranging from zero, at the hygroscopic point (s_h), to a maximum evaporation rate, E_w, at s_w. ET reaches the potential evapotranspiration value (PET) when soil moisture is above a critical value, s^*, comprised between s_w and the field capacity (s_{fc}), which represents incipient stomatal closure based on plant and soil types. For s below s^*, plants enter a water-stressed state, reducing their water use. This is modelled, considering ET constant and equal to PET, when s is higher than s^*, while for s lower than s^*, a linear variation from E_w at s_w to PET at s^* is assumed.

When s exceeds s_{fc}, soil water loss by gravity is triggered. This leakage process is simulated in ECO-PRO by Eq. (6). More specifically, the leakage rate is modelled exponentially (Clapp and Hornberger, 1978), reaching a maximum value, equal to the saturated hydraulic conductivity (k_{sat}), at saturation ($s = 1$), and decreasing as soil dries, following the decay of hydraulic conductivity. An exponent $\beta = 2b + 4$ is considered, where b is the soil pore size and distribution index. Generated leakage is assumed instantaneously transferred to the BL. To avoid leakage overestimation from non-linear effects (Manfreda et al., 2005), ECO-PRO calculates leakage every 10 min and averages it hourly.

2.2.2. Water balance equation for the Blue Layer

The leakage (L) and surface runoff (R) contributions from the GL are diverted into the BL, increasing its water level (h), whose dynamics are modelled by the second relationship in Eq. (1). Water stored in the BL may be lost through direct evaporation (E_b), capillary rise (U_s) or outflow (OUT). Direct evaporation ($E_{b,i}$) occurs only when rainfall is absent, and is calculated by scaling $E_{w,i}$ by a factor α_e, which is a model parameter, ensuring it does not exceed h_i. Considering the Polder Roof's control weir geometry, the outflow term is computed through the equation for a contracted rectangular pivot weir (Aydin et al., 2011), implemented in the *Innovyze H20Calc* of the US EPA SWMM5 (available from the EPA's website: http://www.epa.gov/ednnrmrl/models/swmm/index.htm):

$$Q_i = \begin{cases} 0 & \text{for } H_i \le p_i \\ \alpha_{w,i} \cdot \left(0.4 + 0.05\frac{H_i}{p_i}\right) \cdot \sqrt{2g} \cdot (W - 0.2\,H_i) \cdot H_i^{3/2} & \text{for } H_i > p_i \end{cases} \quad (7)$$

where: Q_i (m^3/s) is the discharge; p_i (m) is the height of the weir crest, which could vary with the weir regulation as a function of the weir closure degree, $c_{dr,i}$; H_i (m) is the head over the weir crest, given by the difference between the water level h_i and p_i (Fig. 2b); g is gravitational acceleration; W (m) is the weir width, with the term $(W - 0.2\,H_i)$ that represents the effective width considering lateral contractions; and, finally, $\alpha_{w,i}$ is a correction factor accounting for the weir inclination, which varies with $c_{dr,i}$. Specifically, this last is obtained considering a linear variation of $\alpha_{w,i}$ from 1, when the weir is fully open (i.e., $c_{dr,i} = 0$) to a maximum value, α_s, which is a model parameter, when the weir is fully closed (i.e., $c_{dr,i} = 1$). It is worth emphasizing that during the entire monitoring period the weir was not subject to regulations and, thus, $\alpha_{w,i}$ was constant and equal to α_s. Analogously to what assumed for the leakage computation, to prevent overestimations, hourly outflow values were calculated by finite differences at a 10-min resolution, capturing the progressive water level changes within each hour; hourly outflow OUT_i (expressed in terms of runoff in mm) is derived from the cumulative water level reduction in an hour with respect to the initial value h_i, assuming it results solely from discharge through the weir during outflow occurrences.

2.3. Dataset of analysis

The reference period considered in this study spans a total of 1287 days (from 12/22/2020 to 06/30/2024). Rainfall data was primarily sourced from the weighing pluviometer, using disdrometer and tipping-bucket gauges data to replace occasional gaps, prioritizing the former, when present, in order to consider data at the maximum possible resolution. Hourly irrigation volumes, available for the entire period, were converted into depth (mm) to obtain the I_{rr} time series. The hourly series of *PET* was derived through the FAO59-PM equation (Allen et al., 1998), leveraging local atmospheric variables at 0.1° × 0.1° spatial resolution from the ERA5-Land reanalysis, according to the methodology adopted and validated in Sicily by Ippolito et al. (2024).

A total of 185,328 continuous hourly outflow measurements (OUT_{obs}) are also available for the entire period and used to assess model performances and drive model parameter calibration, alongside soil moisture observations, available from the end of 2023. The soil moisture dataset, depicted in Fig. 3, includes 3411 measurements of mean areal absolute soil moisture data (θ_{obs}) from two sources: 3382 continuous data (black line in Fig. 3) from WCR sensors (i.e., from 02/05/2024 to 06/30/2024, with a 5-days gap in March due to sensors maintenance operations), and 29 sporadic measurements (black circles in Fig. 3) from the TDR device (i.e., periods after Dec. 2023 without WCR data availability). In Fig. 3, values derived from TDR and not used (red circles) are also reported to highlight how discrepancies between WCR and TDR data were minimal, confirming consistency in soil moisture measurements.

The Full dataset was split into two subsets: approximately 70 % of data, covering a period from 01/09/2022 to 06/30/2024 including the full series of soil moisture observations, was used for Calibration, while the remaining data, corresponding approximately to the first year, were exclusively used for Validation.

2.4. Model parameterization

Model requires to preliminarily set some contour and initial conditions, listed in Table 1a. Contour conditions describe the system's configuration, and include drainage area (A), mean soil depth of the GL (Z_r), BL height (BLH), and weir length (W). Initial conditions for numerical simulations include initial interception storage capacity (c_0), relative soil moisture (s_0) and BL water level (h_0). Model, for both calibration and validation, was initialized on winter days, shortly after outflow events, reasonably assuming a null c_0, soil moisture at field capacity (i.e., $s_0 = s_{fc}$), and initial water level equal to the weir height (i.e., $h_0 = 80$ mm), indicating a full BL. A one-week warm-up period was also neglected from performance evaluations to mitigate the impact of initial condition inaccuracies on calibration and validation.

The model involves 12 parameters, listed in Table 1b. Soil properties are characterized through porosity (n), saturated hydraulic conductivity (k_{sat}), coefficient β for the hydraulic conductivity law, field capacity (θ_{fc}) and plant available water content ($p.a.w.$), which enables to estimate soil moisture at the wilting point, θ_w, from field capacity (i.e., $\theta_w = \theta_{fc} - p.a.w.$). The relative soil moisture points characterizing the water retention curve (s_h, s_w, s^*, and s_{fc}) are calculated based on parameters θ_{fc}, $p.a.w$, n and two scaling parameters: sc_{sh} and sc_{s^*}. The former allows to estimate s_h and is given by the ratio $(s_h\text{-}s_{h,\min})/(s_w\text{-}s_{h,min})$, where $s_{h,min}$ is a lower constrain for the hydroscopic point, assumed equal to that associated with the minimum hydroscopic soil moisture retrievable from literature, $\theta_{h,min}$, fixed as contour condition (Table 1a). A null value for sc_{sh} implies $s_h = s_{h,min}$, while $sc_{sh} = 1$ sets $s_h = s_w$. The parameter sc_{s^*} is given by the ratio $(s^*\text{-}s_{fc})/(s_{fc}\text{-}s_w)$, and allows for estimating the incipient stomatal closure point, s^*, once determined s_w and s_{fc}. A null value for sc_{s^*} sets $s^* = s_w$, while $sc_{s^*} = 1$ implies $s^* = s_{fc}$. This approach to soil parametrization was selected to fit information typically available during the preliminary soil selection for GR installations, and it always ensures the

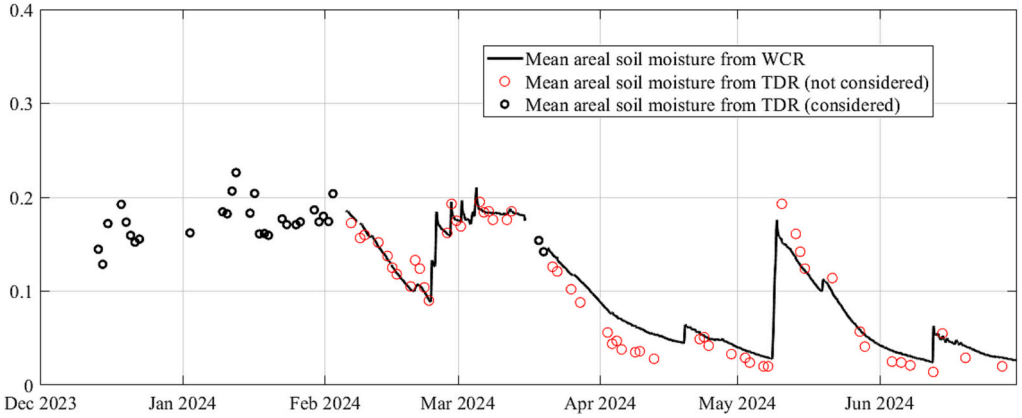

Fig. 3. Hourly time series of mean areal absolute soil moisture (θ_{obs}). Solid black line refers to data derived from WCRs, fully considered in this study. Black circles refer to further spot data derived using a portable TDR and considered in periods without WCR data. Red circles refer to TDR data not considered since acquired in periods already covered by WCR data.

Table 1
Contour and initial conditions (a). Calibration parameters, with indication of the Literature Parameter Set (LPS), the range of variation for each parameter explored in calibration (LRs), and the Optimized Parameters Set (OPS) values (b).

a) Contour and initial conditions

Description	Symbol	Value	Unit
Drainage area	A	32.1	m^2
Mean soil depth (GL)	Z_r	156.1	mm
Height of the BL	BLH	100	mm
Length of the weir	W	500	mm
Max inclination of the weir	ψ	45	°
Max heigh of the weir	p_{max}	80	mm
Initial interception storage capacity	c_0	0	mm
Initial relative soil moisture in the GL	s_0	s_{fc}	–
Initial water level into the BL	h_0	80	mm
Min soil moisture at the hygroscopic point	$\theta_{h,min}$	0.005	–

b) Model calibration parameters

Description	Symbol	Unit	LPS	LRs		OPS
				min	max	
Veg. threshold for canopy interception	Δ	mm	1.00	0.30	1.70	0.70
Max. correction factor for the weir slope	α_s	–	1.20	1.00	1.40	1.37
Mean daily evaporation	$E_{w,day}$	mm/d	0.10	0.03	0.17	0.10
Parameter for the capillary rise model	CS	–	100.0	30.0	170.0	147.3
Soil porosity	n	–	0.55	0.35	0.70	0.61
Scaling coef. for the hygroscopic point	sc_{sh}	–	0.50	0.00	1.00	0.37
Plant available water content	$p.a.w.$	–	0.12	0.05	0.20	0.18
Scaling coef. for the incip. stom. closure point	sc_{s*}	–	0.75	0.00	1.00	0.78
Soil moisture at field capacity	θ_{fc}	–	0.18	0.15	0.25	0.20
Coef. for water retention curve	β	–	3.40	0.18	11.00	4.91
Saturated hydraulic conductivity	k_{sat}	mm/h	6000	3800	8000	6099
Scaling coef. for the evaporation from the BL	α_e	–	0.25	0.01	0.50	0.26

condition of $s_{h,min} \leq s_h \leq s_w \leq s^* \leq s_{fc} \leq 1$, reducing consistently the hyperspace of possible solutions for parameters calibration.

Other model parameters are: the vegetation threshold Δ for interception; the parameter CS of the capillary rise module (Eq. (3)); the maximum value of the weir slope correction factor, α_s (Eq. (7)); the mean daily evaporation $E_{w,day}$; and, the scaling factor α_e, for calculating direct evaporation from the BL ($E_{b,i}$). In particular, it is assumed that the hourly variability of the evaporation E_w follows that of PET, with the parameter $E_{w,day}$ equal to the long-term mean daily evaporation. Thus, staring from the hourly PET series, the model derives hourly $E_{w,i}$ at the generic time i as $E_{w,i} = (E_{w,day}/24)\cdot PET_i/\langle PET\rangle$, where $\langle PET\rangle$ is the average hourly PET over the reference period.

An initial parameter set (referred to as LPS, "*literature parameters set*") and the variability ranges for each parameter (LRs, "*literature ranges*") were first defined based on available information on the experimental site and relevant literature (Table 1b). During the MGR installation, soil data indicated porosity, n, between 0.40 and 0.68, and $p.a.w.$ between 0.06 and 0.18. Such ranges, slightly enlarged (Table 1b), were considered for the LRs. They are consistent with other studies (Chow, 1964; de Munck et al., 2013; Li and Babcock Jr., 2016), some of which specific for GRs volcanic substrates (Stanić et al., 2019, 2020), which also provided useful information for the preliminary setting of other soil parameters and their LRs, such as k_{sat}, β, θ_{fc}, sc_{sh} and sc_{s*}. The soil moisture characteristic points of the water retention curve for the LPS, especially with regards to θ_{fc}, were also verified through the combined analysis of soil moisture and outflow records, considering that outflow is triggered by an increase in the BL water level over the weir height, indicative in turn of leakage occurrences, generated when soil moisture exceeds the field capacity.

The LPS values for the parameters Δ and $E_{w,day}$ were estimated based on values typically adopted in ecohydrological models for grass vegetation (Rodriguez-Iturbe and Porporato, 2004), while the parameter CS was fixed equal to default value used in the *wflow_sbm model*. For these three parameters (Δ, $E_{w,day}$, and CS) a wide variation range (±70 %) was considered for LRs (Table 1b). The scaling factor α_e was initially set to 0.25 for the LPS, that is the midpoint of its expected range variation, assumed from 0.01 to 0.50. This assumption arises from the consideration that the BL is permanently in shaded conditions, thermally insulated by the upper GL, and with reduced wind effects and air movements; all this likely implies a significantly reduced BL evaporation rate compared to the GL direct evaporation. Considering that for the experimental site the weir slope at the maximum closure is 45°, the weir inclination correction factor, α_w, was set to 1.2 for the LPS, based on studies (Bijankhan and Ferro, 2018; Di Stefano et al., 2018) indicating values from 1 to 1.4 (range used for defining the LR for α_s), with the highest values corresponding to weir inclinations between 30°-50°.

2.5. Calibration procedure and performance indicators

The optimization of the LPS within the LRs defined in Table 1b was conducted using a genetic algorithm, resulting in the Optimal Parameter Set (OPS) reported in the same table. Notably, most OPS values were close to those in the LPS, supporting the accuracy of initial parameter estimates.

The genetic algorithm was implemented using the Global Optimization Toolbox of MATLAB, with default settings. A performance Global Index (GI) was defined ad-hoc and used as objective function: it is a weighted average of four dimensionless error indices, each ranging from 0 (perfect matching) to 1 (poorest matching), thus preserving the same range and interpretability. Specifically, the GI is defined by the following equation, whose constituent terms are explained in what follows:

$$GI = \frac{\frac{w_1}{2}\cdot\delta_{out} + \frac{w_1}{4}\cdot PAE_{vol} + \frac{w_1}{4}\cdot PAE_{fr} + w_2\cdot\delta_s}{w_1 + w_2} \tag{8}$$

Each index in Eq. (8) is derived by comparing simulated and observed variables over a reference period (e.g., Calibration, Validation or Full period). The indices δ_{out} and δ_s refer to the one's complement of the Willmott's index (Willmott et al., 2012), which measures alignment between observed and simulated hourly series for outflow and relative soil moisture, respectively. The index for each variable, δ_{var} (with $var = OUT$ for outflow or s for relative soil moisture) is defined by:

$$\delta_{var} = \frac{\sum_{k=1}^{n_{var}} (SIM_k - OBS_k)^2}{\sum_{k=1}^{n_{var}} (|SIM_k - \overline{OBS}| + |OBS_k - \overline{OBS}|)^2} \tag{9}$$

where n_{var} is the sample size, SIM_k and OBS_k are simulated and observed hourly value at the generic time step k, and $\overline{OBS}$ is the average observed value over the reference period. This index was chosen due to its reduced sensitivity to outlier driven errors.

The PAE_{var} indices (PAE_{vol} and PAE_{fr}) represents the Percentage Absolute Error in total outflow volume and frequency of not-null outflow (i.e., $OUT_i > 0.1$ mm), respectively. The general formula for these indices is:

$$PAE_{var} = \frac{|SIM_{var} - OBS_{var}|}{OBS_{var}} \tag{10}$$

where SIM_{var} and OBS_{var} are simulated and observed value for either cumulative outflow volume (*vol*) or frequency of not-null outflow (*fr*), respectively. An upper bound caps the PAE_{var} indices at one, so that all candidate solutions for calibration (i.e., parameters set) with errors exceeding observed values are equally deemed ineffective (i.e., $PAE_{var} = 1$).

For evaluating model performance by the GI, outflow and soil moisture reproduction are weighted differently based on observation coverage. The weights, w_i, in Eq. (8) reflect the proportion of the reference period with available data for outflow (w_1) and relative soil moisture (w_2). They can range from 0 (no data available) to 1 (full period coverage). Moreover, outflow is represented in GI by three different indices (δ_{out}, PAE_{vol} and PAE_{fr}), with δ_{out} weighted at $w_1/2$ and the other two at $w_1/4$ each.

This approach allows GI computation when at least partial data for either variable (outflow or relative soil moisture) are available. Although robustness of GI increases with data availability and improves when measurements for both variables are available, the index does not lose generality if observations for one variable are missing. Additionally, other well-known indicators, including the Root Mean Squared Error (RMSE) and coefficient of determination (R^2), are applied in this study to further assess model accuracy.

2.6. Sensitivity and uncertainty analyses

A sensitivity analysis was performed to evaluate the influence of input variations on output predictions and assess the relative importance of each parameter. Specifically, a Perturbation-based Sensitivity Analysis (PSA) was applied to three outputs: absolute soil moisture θ, water level h, and outflow *OUT*. The analysis involved repeating the following steps for each output, parameter x_j of Table 1b (with $j = 1, 2, \ldots, 12$), and across 100 perturbation ratios ε_k (where $k = 1, 2, \ldots, 100$), from −25 % to +25 % with increments of 0.5 %:

1- Calculation of the output Y_i time series (with Y_i representing θ_i, h_i, or OUT_i, and i referring to the generic hour of the Full period) using the OPS values, and determination of the average value ($\overline{Y}$).
2- Perturbation of each parameter, x_j, by ε_k to create a perturbated input set, $X_j^{pert,k}$, where all parameters are at their optimal values (OPS) except for the j-th parameter, which is modified as:

$$x_j^{pert,k} = OPS_j + \varepsilon_k \cdot OPS_j \tag{11}$$

3- Model simulation using $X_j^{pert,k}$ to compute the perturbated output time series, $Y_j^{pert,k}$.
4- Calculation of the mean sensitivity, $S_{j,k}$, for each parameter-perturbation ratio pair, as:

$$S_{j,k} = \frac{1}{N}\sum_{i=1}^{N}\left|\frac{Y_{j,i}^{pert,k} - Y_i}{\varepsilon_k \cdot \overline{Y}}\right| \tag{12}$$

where N is the total number of hours in the Full period.

Sensitivity results across all perturbation ratios and parameters were aggregated and analyzed by output type.

Model uncertainty was evaluated using a Monte Carlo (MC) method to estimate epistemic uncertainty (i.e., uncertainty in the estimate of model parameters) at a 95 % confidence level. Uncertainty was assessed by quantifying the variability in hourly time series of s, h and *OUT*, based on multiple realizations of uncertain model parameters. This involved generating 10,000 parameter sets by randomly sampling each parameter from a uniform distribution within ±5 % of its OPS value (Table 1b).

Table 2
Comparison between the observed (Obs.) hydrological response and that simulated (Sim.) using the LPS and OPS (Table 1b). Comparison refers to the Calibration, Validation and Full periods and reports the mean annual rates of input forcings (Rainfall, Irrigation and Reference Evapotranspiration) and computed water fluxes (mm/y). Performance indices are reported in the bottom section. Some observed values are not available (*n.a.*), and Willmott's Index ($1\text{-}\delta_s$) for the Validation period is not computable (*n.c.*) due to the lack of observed data. The values of the reconstructed observed actual evapotranspiration from the system (AET_{obs}) are highlighted in bold.

			Reference period								
			Full period			Calibration			Validation		
			Obs.	*Sim.*		*Obs.*	*Sim.*		*Obs.*	*Sim.*	
				LPS	OPS		LPS	OPS		LPS	OPS
Model input											
Mean Annual Rainfall	P	mm/y	582			470			845		
Mean Annual Irrigation	I_{rr}	mm/y	160			153			176		
Mean Annual Ref. Evapotranspiration	PET	mm/y	1170			1189			1125		
Model output											
Mean Annual Canopy Interception	I	mm/y	n.a.	26	24	n.a.	25	22	n.a.	30	27
Mean Annual Act. Evapotransp. - GL	ET	mm/y	n.a.	548	592	n.a.	519	569	n.a.	617	644
Mean Annual Evaporation - BL	E_b	mm/y	n.a.	9	7	n.a.	9	7	n.a.	9	6
Mean Annual Evapotransp. - MGR	AET	mm/y	**619**	583	622	**584**	553	599	**700**	655	677
Mean Annual Leakage	L	mm/y	n.a.	347	323	n.a.	253	225	n.a.	568	552
Mean Annual Capillary rise	U_s	mm/y	n.a.	174	188	n.a.	166	182	n.a.	193	202
Mean Annual Outflow	OUT	mm/y	123	169	140	38	85	53	321	366	344
Performances											
% hours with outflow > 0.1 mm/h	$PR_{OUT,h}$	%	1.8 %	1.8 %	1.4 %	1.2 %	1.1 %	0.7 %	4.0 %	3.4 %	3.3 %
% days with outflow > 2 mm/d	$PR_{OUT,d}$	%	3.3 %	4.5 %	3.6 %	1.2 %	2.8 %	1.7 %	8.4 %	8.6 %	8.1 %
Root Mean Square Error - Hourly OUT	$RMSE_{OUT}$	mm/h	–	0.19	0.18	–	0.12	0.09	–	0.30	0.30
Coefficient of determination, Daily OUT	R^2_{OUT}	[−]	–	0.86	0.88	–	0.68	0.80	–	0.90	0.89
Willmott's Index- hourly soil moisture	$1\text{-}\delta_s$	[−]	–	0.90	0.96	–	0.90	0.96	–	n.c.	n.c.
Global Index	GI	[−]	–	0.49	0.42	–	0.65	0.45	–	0.46	0.46

3. Results

3.1. Model performances

The model was applied to the case study, considering both LPS and OPS parameter sets and comparing the simulated and observed hydrological responses of the system over the Calibration, Validation and Full periods.

Table 2 presents a comparison of mean annual rates of water fluxes across these periods and the associated performance indicators, including: the percentage of hours ($PR_{OUT,h}$) and days ($PR_{OUT,h}$) with significant outflow, assuming 0.1 mm/h and 2 mm/d as lower bounds for defining significant hourly and daily outflow, respectively; the RMSE for hourly outflow ($RMSE_{OUT}$ in mm/h); R^2 for daily outflow (R^2_{OUT}); the Willmott's index for hourly relative soil moisture (1-δ_s); the *GI* used for model calibration.

Both LPS and OPS parameterizations produced similar water fluxes across all periods, despite a marked climate variability (Table 2), indicating a certain stability of model outputs with respect to variations in climate forcings. Simulated hydrological responses also matched satisfyingly the observed behaviour in terms of frequency and magnitude of generated outflow, soil moisture profiles (when available), and annual actual evapotranspiration from the system (*AET*). Simulated *AET* was computed as the sum of actual evapotranspiration from the GL, canopy interception and evaporation from the BL (i.e., $AET_{sim} = ET + I + E_b$), while observed *AET* was estimated through long-term water balance (i.e., $AET_{obs} = P + I_{rr}\text{-}OUT_{obs}$), reasonably assuming a negligible variation of water storage into the GL and BL at the end of the reference period with respect to other terms.

Compared to the LPS, the OPS achieved a more accurate reproduction of the mean annual outflow in all the examined periods, with percent error of 14 % over the Full period (vs. 38 % using the LPS) corresponding to an error of only 27 mm/y. All performance indicators for daily outflow demonstrated for the OPS superior performance over the Full and Calibration periods compared to LSP, and similar performances over the Validation period. For instance, especially over the Calibration period, the model with the OPS provided an accurate reproduction of the outflow frequency, resulting in lower errors in $PR_{OUT,d}$ and a higher R^2_{OUT} than the LPS. The $PR_{OUT,h}$ values denoted for all periods a slightly higher capacity of the model in reproducing the frequency of significant hourly outflow with the LPS rather than using the OPS; however, the lower $RMSE_{out}$ values obtained with the OPS confirms that this last outperforms the LPS also in terms of hourly outflow reproduction.

In terms of *AET*, the OPS slightly outperformed LPS across all periods, with a negligible error (+0.5 %, corresponding to 3 mm/y) over the Full period. The values of Willmott's index were notably high with both parameterizations (i.e., 0.90 with LPS and 0.96 with the OPS for both periods with available soil moisture records), underscoring model's ability in capturing soil moisture dynamics during both Calibration and Full periods.

A visual comparison over the Full period between model outputs with the OPS and observed values is reported in Fig. 4, which shows daily time profiles of water input ($P + I_{rr}$) in mm/d, absolute soil moisture θ (−), BL water level (mm), and outflow (mm/d). Simulated soil moisture dynamics strongly reflect seasonal patterns driven by water input, as it was expected given the relatively small thickness of the GL and the strong climate seasonality. The comparison with observed soil moisture (red markers in figure) during the last period confirm the model's effectiveness in capturing both rapid wetting and slower drying phases and supports the results of the optimization of the soil parameters characterizing the water retention curve.

The simulated time profiles of BL water level exhibited a seasonal alternance in water storage, coherently with observed soil moisture traces in the GL, as water enters the BL via leakage. The BL dryness rates varied seasonally: during the wet-cold season, drying rates were low due to reduced atmospheric and plant water demand, while during the spring-summer period, which is also the growing season for vegetation, drying processes were more rapid. Over the Full period, consistently with evidence from periodic on-site visual inspections of the BL, ECO-PRO predicted annually a period in the summer with BL completely empty, lasting at least 30 consecutive days. The possibility of a dynamic assessment of water storage into the BL is valuable for the MGR management, as it allows for evaluating at any time the available water

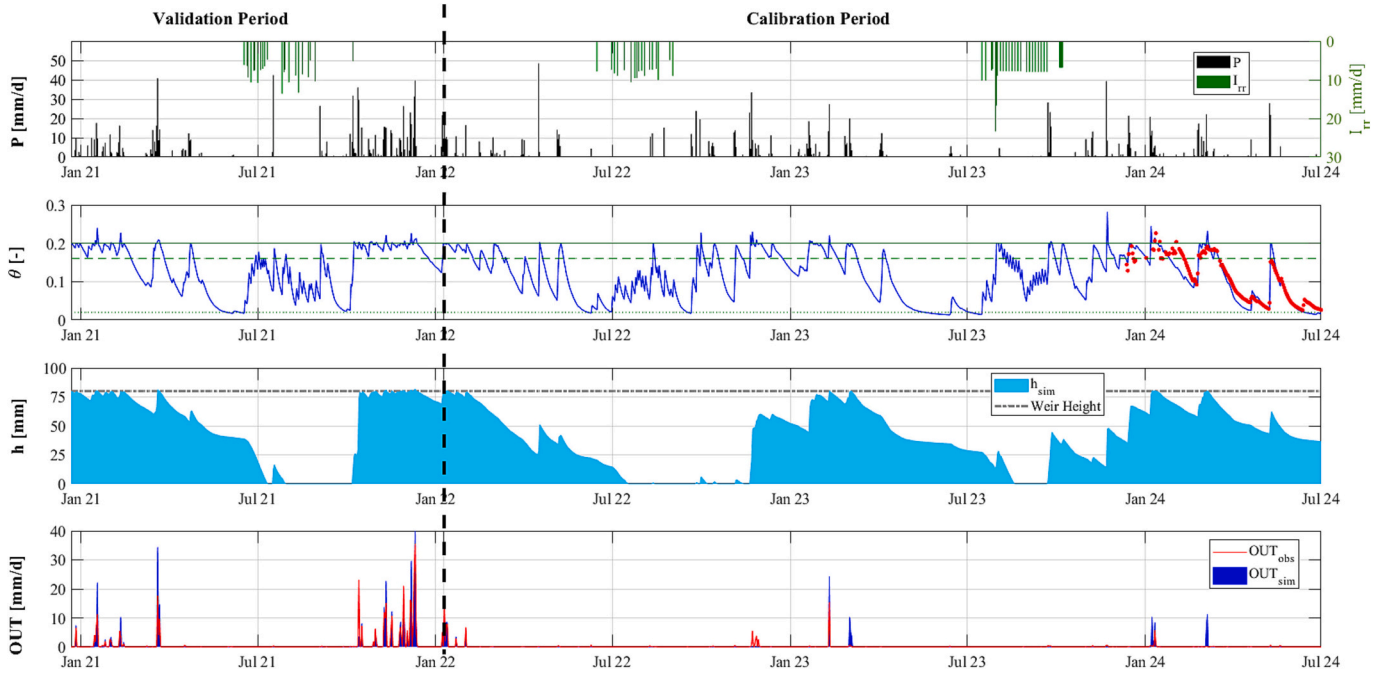

Fig. 4. Daily time series of rainfall (*P*) and irrigation (I_{rr}) in the top plot. Observed (red markers) and simulated (blue line) mean absolute soil moisture, θ, in the upper-middle plot, where the characteristic soil moisture values (θ_w, θ^*, and θ_{fc}) are also depicted by horizontal green lines. Mean water level into the blue layer, *h*, and weir height (dashed grey line) in the lower-middle plot. Simulated (OUT_{sim}) and observed (OUT_{obs}) outflow in the bottom plot.

resources for reuse and the residual stormwater retention capacity of the system, which is crucial for mitigating extreme rainfall.

Although BL water levels were not systematically monitored, the model's reliability in simulating them is supported by its demonstrated accuracy in predicting outflows, which occur only when water levels exceed the weir height. The bottom plot in Fig. 4 shows that the model closely reproduced the timing of most significant outflow events, with slight discrepancies, especially in some peaks reproduction, potentially due to measurement inaccuracies. Some observed anomalies, such as isolated small outflows during summer when the BL was empty, may arise from sporadic and undesired rainfall infiltrations in the zone of connection of the MGR with the draining system that convey outflow toward the external rain barrel, where outflow is measured; this could lead to possible overestimations of observed occurrences of small outflow values and, to a lesser extent, of the observed outflow volumes.

3.2. Model's sensitivity to parameters and epistemic uncertainty

The sensitivity analysis, following the procedure in Section 2.6, assessed the model's response to variations in input parameters for soil moisture (Fig. 5a), water level (Fig. 5b) and outflow (Fig. 5c). Mean sensitivity values ($S_{j,k}$) above one indicate high model sensitivity to the j-th parameter, signifying that the mean percent variation in the output exceeds the imposed perturbation rate (ε_k). Parameters with higher $S_{j,k}$ are the most influential on the model's output in relative terms.

Overall, the PSA revealed low sensitivity across all outputs, with most parameters showing $S_{j,k}$ under 0.10 across the full perturbation range. Among the outputs, soil moisture showed the highest sensitivity to parameter changes (Fig. 5a), with $S_{j,k}$ values exceeding one only for field capacity (θ_{fc}) and porosity (n). Another influential parameter on soil moisture is *p.a.w.*, whose sensitivity was however in the order of 0.5. Except for sc_{s*} and *CS*, having $S_{j,k}$ values in the order of 0.25, soil moisture is essentially not sensitive to all other parameters, with $S_{j,k}$ values generally below 0.03.

Water level, h, and outflow, *OUT*, displayed minimal sensitivity to parameter variations. Specifically, the most influential parameters for h (Fig. 5b), with $S_{j,k}$ in between 0.25 and 0.5, are *p.a.w.*, *CS*, and, to a lesser extent, sc_{s*}. Sensitivity for h to other parameters never exceeded 0.05. Outflow sensitivity (Fig. 5c) was most strongly affected by α_s, *p.a.w.* and, in a lower measure, by sc_{s*} and *CS*, showing however $S_{j,k}$ values approximatively between 0.15 and 0.5. Except for $E_{w,day}$, having sensitivity of 0.05, outflow predictions resulted essentially not sensitive to variations in the remaining parameters.

The PSA results show symmetric model response to positive and negative perturbations, suggesting no directional bias. Slight descendent trends in $S_{j,k}$ for increasing ε_k (from −25 % to 25 %) can be noticed only for the most influential parameters of each output, with the only exceptions for the sensitivity to θ_{fc} and sc_{s*} that exhibit slight increasing trends. However, sensitivity remained generally constant for small perturbations (−5 % to +5 %) across different perturbation levels (Fig. 5).

Fig. 6 summarizes the results of the uncertainty analysis conducted according to the procedure in Section 2.6. Figure shows the variability in each model output (i.e., relative soil moisture, water level and outflow) within the fixed confidence interval, reporting the mean prediction and the 95 % confidence band (i.e., delimited by the 2.5th and 97.5th percentile) of all the realizations considered. In the bottom graph, inset plots reporting a zoom for some outflow events are also depicted for helping visualization. Results show limited impact of parameter uncertainty on model reliability, with the greatest output variability appearing during decay phases of soil moisture and water level, while recharge phases displayed narrower uncertainty bands, indicating greater robustness in the model's predictions. Outflow was the least affected output by parameter uncertainty, reflecting the process's dependence on

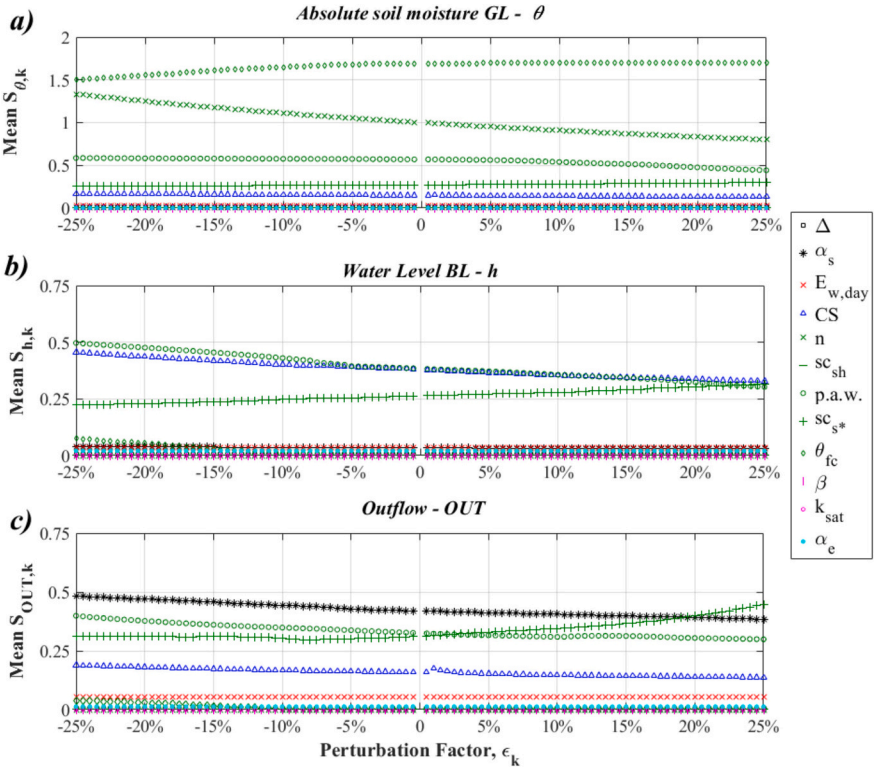

Fig. 5. Perturbation-based Sensitivity Analysis (PSA) of model outputs to its parameters (symbols are the same as Table 1b). The PSA is conducted across 100 perturbation ratios, ε_k (from −25 % to +25 %). The Mean Sensitivity, $S_{j,k}$, for an output to the generic j-th parameter associated with the k-th perturbation ratio is computed by Eq. (12). The $S_{j,k}$ values are depicted as a function of ε_k using different colored markers depending on the considered parameter. The sensitivity is analyzed separately for each output: (a) absolute soil moisture, θ, in the Green Layer (GL); (b) water level, h, into the Blue Layer (BL); (c) outflow, *OUT*.

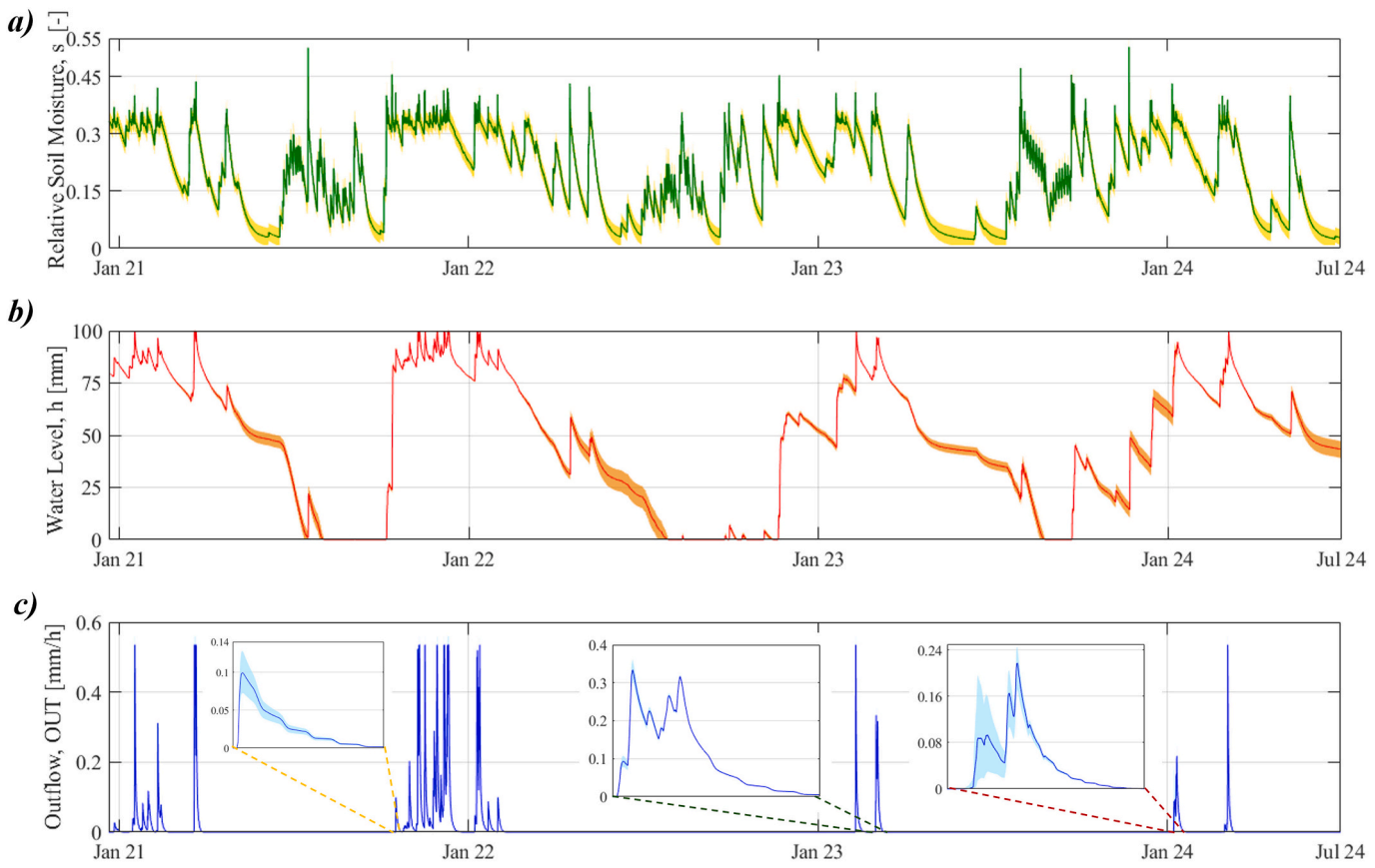

Fig. 6. Uncertainty analysis for ECO-PRO: a Monte Carlo based approach, considering 10,000 realizations and a ±5 % uncertainty range of the parameters around the OPS (Table 1b), was used to propagate uncertainties in parameters through the model and quantify the effects on simulated hourly time series of: (a) relative soil moisture, s (−); (b) water level into the BL, h (mm); and (c) outflow, OUT (mm/h). The mean predictions and the 95 % confidence bands are depicted for each output. Inset plots in the bottom graph, report a zoom over periods of duration from 9 to 14 days for three outflow events.

high soil moisture in the GL and water levels in the BL exceeding the weir height, typically following recharge phases. However, significant changes in outflow traces can occur for low-magnitude outflow events, while the model response appears much more stable for the most severe events, as can be noticed from inset plots in Fig. 6. Overall, model's predictions for timing and duration of significant outflow events remain stable under the explored parameter uncertainty range (±5 % around the OPS values).

Table 3
Selected Prolonged Rainy Spells (PRSs) generating outflow according to the model. Assigned identification number (*ID*), start date, total cumulative rainfall (P_{tot}), rainfall duration (*dur*) and mean intensity ($\langle I_{nt} \rangle$) for each PRS. Outflow observed (OUT_{obs}) and simulated (OUT_{sim}) during each PRS and corresponding observed (SRR_{obs}) and simulated (SRR_{sim}) Stormwater Retention Rate (OUT_{obs} and SRR_{obs} values are reported in italics). Relative percentage contribution to the SRR of the Green Layer (GL) and Blue Layer (BL) for each PRS. Bottom row reports mean values across all PRSs (in bold italics).

		P_{tot}	*dur*	$\langle I_{nt} \rangle$	OUTFLOW [mm]		SRR [−]		Contr. to SRR [%]	
ID	Start date	[mm]	[d]	[mm/d]	OUT_{obs}	OUT_{sim}	SRR_{obs}	SRR_{sim}	GL	BL
1	December 27, 2020	14	2	6.9	*6.5*	7.4	*0.53*	0.46	31.5 %	68.5 %
2	January 16, 2020	37	4	9.3	*24.4*	27.9	*0.34*	0.25	13.3 %	86.7 %
3	February 01, 2021	16	3	5.4	*5.5*	6.3	*0.66*	0.61	30.2 %	69.8 %
4	February 08, 2021	29	5	5.9	*9.0*	10.3	*0.69*	0.65	27.0 %	73.0 %
5	March 19, 2021	91	6	15.1	*31.4*	58.2	*0.65*	0.36	10.5 %	89.5 %
6	October 14, 2021	82	5	16.3	*30.9*	11.7	*0.62*	0.86	3.3 %	96.7 %
7	November 01, 2021	12	2	6.0	*7.7*	8.6	*0.36*	0.29	21.6 %	78.4 %
8	November 07, 2021	57	6	9.4	*37.1*	42.1	*0.35*	0.26	16.3 %	83.7 %
9	November 17, 2021	26	2	13.1	*16.2*	17.8	*0.38*	0.32	36.9 %	63.1 %
10	November 26, 2021	52	6	8.6	*38.7*	41.4	*0.25*	0.20	11.6 %	88.4 %
11	December 06, 2021	43	3	14.5	*32.5*	37.9	*0.25*	0.13	14.1 %	85.9 %
12	December 10, 2021	87	5	17.4	*76.0*	80.5	*0.13*	0.07	10.6 %	89.4 %
13	January 08, 2022	71	7	10.1	*38.2*	39.9	*0.46*	0.44	39.6 %	60.4 %
14	February 09, 2023	42	3	13.9	*15.6*	24.4	*0.62*	0.41	35.8 %	64.2 %
15	February 27, 2023	57	10	5.7	*1.1*	19.1	*0.98*	0.66	34.6 %	65.4 %
16	January 07, 2024	60	8	7.6	*7.6*	21.7	*0.87*	0.64	23.4 %	76.6 %
17	February 29, 2024	48	7	6.8	*0.4*	19.1	*0.99*	0.60	7.7 %	92.3 %
	MEAN	***48***	***5***	***10.1***	***22.3***	***27.9***	***0.54***	***0.42***	***21.6 %***	***78.4 %***

3.3. Model application: Stormwater Retention Rate assessment for prolonged rainy spells

Assessing the hydrological performance of an existing MGR is essential for evaluating its actual functionality, particularly in the absence of an extensive sensor network. This section presents an application of ECO-PRO with this purpose, which also represents a further test on the model. In particular, the retention function of the experimental site in response to various significantly wet sub-periods is reconstructed, analyzing its performance in term of Stormwater Retention Rate, SRR (Carter and Jackson, 2007; Pumo et al., 2023a), which is defined as the fraction of the total incoming water (rainfall plus irrigation if present) retained by the system. By simulating soil moisture and water level into the BL, the model also enables estimation of each layer's contribution to the total retention function of the system.

The analysis was conducted on aggregated daily time series, with a focus on significant wet sub-periods, referred to as Prolonged Rainy Spells (PRSs), which have the potential to generate outflow. Specifically, PRSs were defined as periods with two or more consecutive rainy days, preceded and followed by at least one dry day. The decision to analyze only significantly long and wet sub-periods was primarily driven by the aim of assessing the system's capacity to reduce runoff volumes and store rainwater for potential later reuse. By aggregating rainfall over relatively long PRSs, this approach facilitates an effective evaluation of the retention efficiency under varying initial conditions, which is particularly valuable for optimizing management strategies for blue-green systems. The adopted methodology identified a total of 55 PRSs throughout the full monitoring period.

According to model simulations, only 17 PRSs (Table 3) generated not-null outflow (>0.1 mm), all of which occurred in autumn and winter. On average, these PRSs carried a total rainfall of 48 mm (range: 12 to 91 mm) over a duration of 5 days (range: 2 to 10 days). Simulated outflow in response to these PRSs varied widely, from 6.3 to 80.5 mm (with an average of 28 mm), and the average simulated SRR per PRS (SRR_{sim}) was 0.42.

Model predictions closely aligned with observed data. The 55 selected PRSs accounted for 93 % of the total observed outflow over the Full period, with the 95 % occurring during the PRSs listed in Table 3. Significant outflow was observed for all the 17 PRSs in Table 3; for these PRSs the average observed outflow (22.3 mm) was rather close to that simulated, with an average observed SRR (SRR_{obs}) of 0.54. The model errors across these PRSs were, on average, approximately 6 mm for total outflow and 12 % for SRR.

Simulation results further indicated that retention during such PRSs was largely driven by the BL rather than the GL, with average percent contributions of 78 % from the BL and 22 % from the GL (Table 3). This finding is consistent with the fact that the PRSs prevalently occurred between November and February, a period characterized by wet antecedent conditions and elevated soil moisture levels, which reduced the residual water storage capacity of the GL. The critical influence of storm characteristics (e.g., rainfall depth, duration, and intensity) and antecedent system conditions (i.e., initial soil moisture in the GL and initial water levels in the BL) on the retention capacity of multilayer green roofs was demonstrated in Pumo et al. (2023a), which used hourly monitored data to investigate the system's hydrological response to various individual rainfall events, with an inter-event period of 6 h used to distinguish separate events.

Fig. 7a presents a regression plot comparing SRR_{sim} to SRR_{obs} for the PRSs listed in Table 3, showing satisfactory alignment along the 45° perfect match line and an R^2 of 0.83. When including the remaining 38 PRSs for which model predicted no outflow, the matching degree further improve and R^2 reaches 0.91. Fig. 7b provides a visual representation of all 55 PRSs in terms of cumulative rainfall and duration.

The corresponding hydrological responses for the PRSs in Table 3 and the other PRSs, are presented in Fig. 8a and b, respectively. Observed data confirmed that the 38 PRSs for which the model predicted no outflow either produced no outflow (14 cases) or minimal outflow, exceeding 1.2 mm in only two cases, where outflow reached around 6 mm. Five of these PRSs occurred in winter, six in spring, and the majority were distributed across summer (12 PRSs) and autumn (15 PRSs). The average observed outflow and SRR values for these 38 PRSs were 0.6 mm and 0.98, respectively, remarking the strong retention capacity of the system, which fully retained considerable rainfall (total depth up to 78 mm and mean intensity up to 26 mm/d) over 2 to 10 consecutive days.

Fig. 8b shows that for most PRSs with null or negligible observed outflow (PRSs with ID from 18 to 55), the GL contributed more to the retention function of the system than the BL. For these PRSs, the average relative contributions to the SRR were 61 % from the GL and 39 % from the BL. Notably, for eight PRSs prevalently occurring in summer or early autumn (IDs: 21, 26, 29, 34, 35, 38, 45 and 48), the GL absorbed all incoming rainfall, resulting in negligible changes in the BL water level. This result further emphasizes the significant role of antecedent system conditions and aligns with the findings of the observational study by Pumo et al. (2023a).

This application highlights the potential of the model to dynamically assess the water presence and, consequently, the residual retention capacity of both the GL and the BL at any time. When combined with accurate rainfall forecasts, this information can provide a reliable estimate of the expected total retention function of the system in response to incoming rainfall.

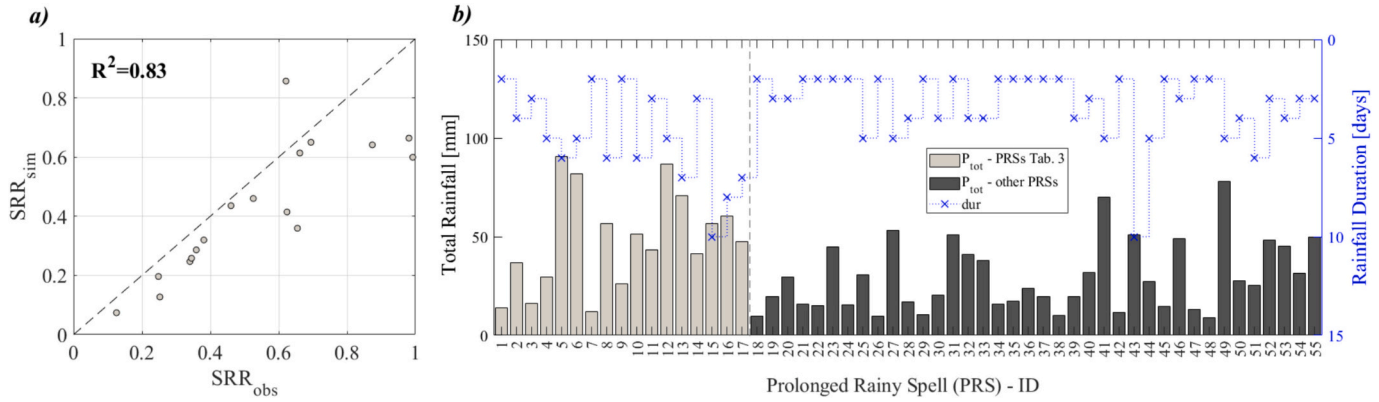

Fig. 7. Regression plot of observed (SRR_{obs}) vs. simulated (SRR_{sim}) Stormwater Retention Rates for the 17 PRSs listed in Table 3(a). Rainfall characteristics (P_{tot} = cumulative rainfall in mm; dur = duration in days) for all 55 PRSs selected, with ID reported in the x-axis (ID for the first 17 PRSs are the same as Table 3). Bars for PRSs included and not included in Table 3 are represented with different color.

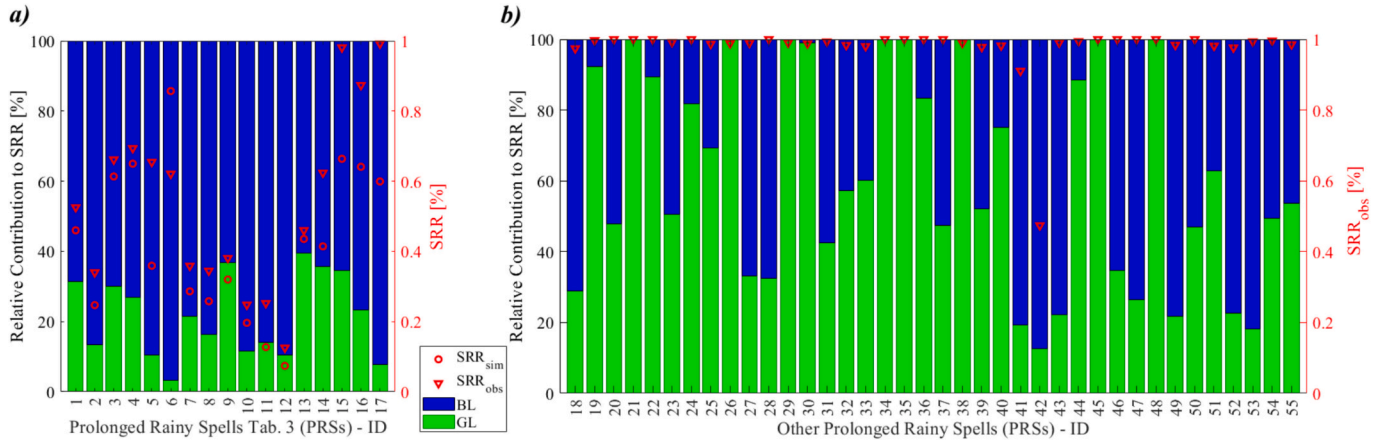

Fig. 8. Relative percent contribution (right y axis) to the system retention function of the Green Layer (GL) and the Blue Layer (BL) for each PRS; red triangles and circles refers to the observed and simulated SRR, respectively, whose values are visualized in the left y-axis. Panel (a) refers to the 17 PRSs listed in Table 3, while other PRSs are visualized in panel (b), where SRR_{sim} are not reported since they are all equal to one.

4. Discussion

Modelling GRs requires simulating interconnected physical and biological processes that drive their functions. Depending on data availability and the specific modelling objectives, such as assessing stormwater retention, energy savings, biodiversity support, or a combination of these factors, different approaches may be appropriate. Modelling MGRs is often focused on assessing hydrological behaviour. This is more complex than for conventional GRs due to the dynamic water exchanges between different layers. Although general-purpose hydrological software (e.g. SWMM, MIKE, HYDRUS, etc.) offers flexible options for simulating urban hydrology and NBSs, they require careful adaptations and simplifications for MGRs (Li and Babcock Jr., 2016). Additionally, these tools face limitations in modelling LID features (Elliott and Trowsdale, 2007; Lee et al., 2012; Burszta-Adamiak and Mrowiec, 2013; Jeffers et al., 2022). SWMM's Low Impact Development (LID) module, for example, provides an oversimplified representation of soil water retention and flow processes, as noted in Baek et al. (2020), whereas HYDRUS is primarily designed for unsaturated soil flow modelling and does not inherently account for the integrated storage and controlled release mechanisms characteristic of MGRs.

Conceptual models based on the water balance theory offer a viable approach to MGR modelling. For instance, Yan et al. (2024) developed a simplified daily model based on a pilot-scale MGR module (1 × 1 m) in a temperate monsoon climate (Beijing, China), validated over a short (around 4 months) period for simulating SRRs.

Expanding on this approach, the current study introduced the ECO-PRO, a novel ecohydrological model for simulating MGRs hydrological behaviour in response to climate conditions. Developed around an advanced MGR under a typical semi-arid Mediterranean climate, ECO-PRO numerically solves a combined GL and BL water balance at an hourly timescale, modelling all water fluxes involved in the balance. The model simulates comprehensively water exchanges between different layers, also accounting for capillary rise and root uptake fluxes, neglected for example in Yan et al. (2024). The proposed model, then, is specifically designed for MGR applications, incorporating a detailed representation of the dynamic water exchanges between the different layers. Additionally, unlike SWMM and HYDRUS, which rely on externally defined boundary conditions for water storage management, our model integrates dynamic storage regulation, enabling a more accurate simulation of retention and controlled outflow processes under varying environmental and operational conditions.

ECO-PRO requires hourly inputs for rainfall and reference evapotranspiration, and can incorporate management functions, such as GL irrigation and weir regulation. While the first aspect was investigated, the second aspect was not tested as the weir remained fixed at maximum closure. Thus, model performances in terms of outflow, and in particular the variable correction factor ($\alpha_{w,i}$) in Eq. (7) associated with the weir closure degree, should be further verified under dynamic weir regulation. Leaving further evaluation of outflow regulation and its impact on outflow hydrographs for future works, it is worth noticing that an imprecise estimate of $\alpha_{w,i}$ may impact hydrograph peaks and base times but likely has minimal influence on hydrograph volume.

ECO-PRO demonstrated consistent accuracy across various timescales and periods (Table 2). Sensitivity analysis revealed that the model is generally stable even when subjected to parameter estimation inaccuracies. Specifically, small parameter perturbations had minimal impact on soil moisture, water levels, and outflow time series. However, soil parameters, such as field capacity and porosity, showed higher sensitivity under larger perturbations, particularly for soil moisture, consistently with what observed in Yan et al. (2024). This behaviour arises because field capacity and porosity define critical thresholds for water storage and drainage, regulating water availability in the GL and its redistribution within the system. When these parameters undergo significant alterations, the soil-water retention curve shifts nonlinearly, amplifying their effects on soil moisture dynamics. This aspect is rather common also using different approaches for modelling green roofs; for instance, a sensitivity analyses conducted in Baek et al. (2020) demonstrated that field capacity and porosity are also the most influential parameters for SWMM Green Roof LID control. This underlines the importance of precise assessment of these easily measurable parameters for accurate soil moisture modelling. Other parameters proved less critical, displaying minimal sensitivity across the various perturbation rates, underscoring ECO-PRO's robustness to parameter uncertainties. This stability was evident when using two similar parameter sets (i.e., LPS and OPS, Table 2). Using the LPS, the model delivered acceptable estimates for all water fluxes (Table 2), demonstrating its suitability also without a complex parameter tuning, such as that considered here, based on sensor-data (not always available) and genetic algorithms.

Further validation through uncertainty analysis (Section 3.2) affirmed that the explored uncertainty level (i.e., parameter variations of ±5 %) is acceptable for the intended uses of the model. This analysis focused on epistemic uncertainty, as ECO-PRO's robust performance across diverse climatic conditions during the Calibration and Validation periods (Table 2) negated the need to address aleatoric uncertainty, related to possible noise in the external forcings. Notably, the model performed consistently over a three-year calibration period with relevant climate variability (Fig. 3), indicating stability across different climatic contexts.

This work showed only one possible "post-implementation"

application of the model (Section 3.3), while ECO-PRO has versatile applications, also concerning pre-implementation analyses for still not realized MGRs. For example, the model can estimate expected hydrological performance for feasibility studies and explore different design configurations, such as drainage area size, layer thickness, and vegetation cover. These insights are crucial for evaluating the cost-effectiveness of design choices. In post-implementation scenarios, ECO-PRO can support dynamic MGR management for various objectives, such as water reuse, rainfall impact mitigating, and climate adaptation. For example, it could guide optimal control of the outflow weir, adjusting it based on current water storage at the different layers and weather forecasts.

ECO-PRO was here subjected to a site-specific calibration, but its modular structure supports wider application. Built in MATLAB, the model allows configuration of initial/boundary conditions and parameters, facilitating adaptation to varied MGR features and climates. Its modular code also enables modification of individual functions (e.g., outflow generation, capillary rise) without altering core equations. For instance, the outflow function should be modified if the control valve differs from that of the experimental site here considered and it is no longer conceptualizable with a contracted rectangular pivot weir.

5. Conclusion

Resilience, sustainability, hydraulic and hydrological invariance are crucial in urban areas heavily impacted by climate change and urbanization. In response, urban development policies are increasingly adopting climate-adaptive design principles. While "green" solutions offer multiple resilience benefits, quantifying these benefits remains challenging, hindering their integration into urban planning through cost-benefit analyses. In this context, modelling plays a crucial role in designing, evaluating, and optimizing these solutions.

Multilayer Green Roofs (MGRs) extend the benefits of traditional green roofs (e.g. UHI attenuation, enhanced thermal and acoustic insulation, biodiversity preservation, etc.) while also buffering extreme rainfall impacts and storing stormwater for reuse. ECO-PRO, a model designed for MGRs, addresses a critical gap, as most existing models are focused on traditional GRs and rely on overly simplified water balance equations.

Despite the limitations highlighted in the previous section, ECO-PRO is efficient, requiring few parameters and displaying minimal sensitivity to inaccuracies in their estimation. It also exhibits low output uncertainty, particularly for outflow predictions, which are critical in MGR applications.

Tested over three years with high-resolution data, ECO-PRO accurately replicated the experimental site's hydrological responses, predicting timing and volume of outflows during significant rainfall events and providing a reliable reproduction of the Stormwater Retention Rates, SRRs, associated with prolonged rainy spells ($R^2 = 0.91$). The model can provide critical insights into seasonal retention dynamics and the contributions of GL and BL to stormwater management. For example, ECO-PRO revealed (Fig. 7) which fractions of rainfall are retained by the green layer (GL) and blue layer (BL) for potential reuse, aiding the evaluation of MGR benefits. The analysis also confirmed that the experimental site can effective manages frequent, small to moderate rainfall events, with most spring-summer rainfall fully retained by the system, mainly exploiting the storage capacity of the GL. In contrast, winter rainfall retention relies more on the BL's residual storage capacity, influenced by management rules. Although direct measurements were unavailable to verify the estimated relative contributions of the GL and BL to the system SRR, the close match between simulated soil moisture profiles and observations (Willmott's index equal to 0.96 over six months with data availability) supports the reliability of such model's partitioning estimates.

The proposed model can facilitate efficient MGR management, even when real-time sensor networks are unavailable. The potential of the model goes beyond the assessment of the hydrological function of a MGR, which was the focus for the demonstrative application presented in this study. ECO-PRO can simulate the full spectrum of water fluxes, including evapotranspiration, whose quantification is essential for assessing UHI mitigation and thermal performance of MGRs. The model's versatility suggests further applications, such as quantifying the impacts of active outflow regulation on stormwater dynamics and testing its adaptability across diverse climates and MGR configurations. Future research could expand on these capabilities, enhancing ECO-PRO's contribution to resilient urban design and sustainable water management.

CRediT authorship contribution statement

Dario Pumo: Writing – review & editing, Writing – original draft, Visualization, Validation, Supervision, Software, Resources, Project administration, Methodology, Investigation, Funding acquisition, Formal analysis, Data curation, Conceptualization. **Matteo Ippolito:** Data curation. **Francesco Alongi:** Data curation. **Antonio Francipane:** Writing – review & editing, Supervision, Data curation. **Leonardo V. Noto:** Writing – review & editing, Supervision, Project administration, Funding acquisition, Data curation.

Funding

This research did not receive any specific grant from funding agencies in the public, commercial, or not-for-profit sectors.

Declaration of competing interest

The authors declare that they have no known competing financial interests or personal relationships that could have appeared to influence the work reported in this paper.

Acknowledgments

This study was carried out within the project CLEVER ("CLimate-changE-resilient cities Via Extensive and Rational use of nature-based solutions", CUP B53D23007540006, Grant 2022SZWBCP) funded by European Union – Next Generation EU, Mission 4, Component C2, Investment 1.1 (PRIN 2022, Call for tender No. 104 published on 2.2.2022 by the Italian Ministry of University and Research). This manuscript reflects only the authors' views and opinions, and the Ministry cannot be considered responsible for them. The experimental prototype was realized within an agreement with Delft University of Technology (Netherlands) as part of the EIT Climate-KIC program (funding received from the European Union Climatic KIC programme with grant number EIT SGA 2018 supporting project 'Polder Roof Fieldlabs - 180522').

Data availability

Dataset that has been used is confidential and can be provided by the authors on request. The model, coded in Matlab, is also available on request from the corresponding author.

References

Allen, R.G., Pereira, L.S., Raes, D., Smith, M., 1998. Crop Evapotranspiration – Guidelines for Computing Crop Water Requirements - FAO Irrigation and Drainage Paper 56. FAO-Food and Agriculture Organization of the United Nations, Rome.

Almeida, A.P., Liberalesso, T., Silva, C.M., Sousa, V., 2023. Combining green roofs and rainwater harvesting systems in university buildings under different climate conditions. Sci. Total Environ. 887, 163719. https://doi.org/10.1016/j.scitotenv.2023.163719.

Andenæs, E., Kvande, T., Muthanna, T.M., Lohne, J., 2018. Performance of blue-green roofs in cold climates: a scoping review. Buildings 8, 55. https://doi.org/10.3390/buildings8040055.

Ávila-Hernández, A., Simá, E., Ché-Pan, M., 2023. Research and development of green roofs and green walls in Mexico: a review. Science of the Total Environment 856 (Part 1), 158978. https://doi.org/10.1016/j.scitotenv.2022.158978.
Aydin, I., Burcu Altan-Sakarya, A., Sisman, C., 2011. Discharge formula for rectangular sharp-crested weirs. Flow Meas. Instrum. 22 (2), 144–151. https://doi.org/10.1016/j.flowmeasinst.2011.01.003.
Baek, S., Ligaray, M., Pachepsky, Y., Chun, J.A., Yoon, K.-S., Park, Y., Cho, K.H., 2020. Assessment of a green roof practice using the coupled SWMM and HYDRUS models. J. Environ. Manage. 261, 109920. https://doi.org/10.1016/j.jenvman.2019.109920.
Bijankhan, M., Ferro, V., 2018. Experimental study and numerical simulation of inclined rectangular weirs. J. Irrig. Drain. Eng. 144 (7). https://doi.org/10.1061/(ASCE)IR.1943-4774.0001325.
Brears, R.C., 2018. Blue and Green Cities: The Role of Blue-Green Infrastructure in Managing Urban Water Resources, 1st ed. Palgrave Macmillan, London, UK.
Burszta-Adamiak, E., Mrowiec, M., 2013. Modelling of green roofs' hydrologic performance using EPA's SWMM. Water Sci. Technol. 68, 36–42. https://doi.org/10.2166/wst.2013.219.
Carbone, M., Garofalo, G., Nigro, G., Piro, P., 2014. A conceptual model for predicting hydraulic behaviour of a green roof. Procedia Eng. 70, 266–274. https://doi.org/10.1016/j.proeng.2014.02.030.
Carter, T., Jackson, C.R., 2007. Vegetated roofs for stormwater management at multiple spatial scales. Landsc. Urban Plann. 80 (1–2), 84–94. https://doi.org/10.1016/j.landurbplan.2006.06.005.
Chow, V.T., 1964. Handbook of Applied Hydrology. McGraw-Hill Book Publishing Company, New York.
Cirkel, D.G., Voortman, B.R., van Veen, T., Bartholomeus, R.P., 2018. Evaporation from (blue-)green roofs: assessing the benefits of a storage and capillary irrigation system based on measurements and modeling. Water 10 (9), 1–21. https://doi.org/10.3390/w10091253.
Clapp, R.B., Hornberger, G.M., 1978. Empirical equations for some soil hydraulic-properties. Water Resour. Res. 14, 601–604.
Cook, L., Larsen, T., 2020. Towards a performance-based approach for multifunctional green roofs: an interdisciplinary review. Build. Environ. https://doi.org/10.1016/j.buildenv.2020.107489.
Cristiano, E., Annis, A., Apollonio, C., Pumo, D., Urru, S., et al., 2022. Multilayer blue-green roofs as nature-based solutions for water and thermal insulation management. Hydrology Research 53 (9), 1129–1149. https://doi.org/10.2166/nh.2022.201.
de Munck, C.S., Lemonsu, A., Bouzouidja, R., Masson, V., Claverie, R., 2013. The GREENROOF module (v7.3) for modelling green roof hydrological and energetic performances within TEB. Geosci. Model Dev. 6, 1941–1960. https://doi.org/10.5194/gmd-6-1941-2013.
Deltares, 2016. Wflow, a Modelling Platform for Hydrological Simulations. Deltares. https://wflow.readthedocs.io/en/latest/index.html (latest access on 04/04/2024).
DHI, 2017. MIKE Urban Collection System - Modelling of Storm Water Drainage Networks and Sewer Collection Systems (User Guide). MIKE Powered by DHI. http://d.g.wanfangdata.com.cn/Periodical_mkhjbh201605010.aspx.
Di Stefano, C., Ferro, V., Bijankhan, M., 2018. Discussion of 'Extraction of the flow rate equation under free and submerged flow conditions in pivot weirs with different side contractions' by N. Sheikh Rezazadeh Nikou, M. J. Monem, and K. Safavi. J. Irrig. Drain. Eng. 144 (4), 07018008. https://doi.org/10.1061/(ASCE)IR.1943-4774.0001249.
Elliott, A.H., Trowsdale, S.A., 2007. A review of models for low impact urban stormwater drainage. Environ. Model. Software 22 (3), 394–405. https://doi.org/10.1016/j.envsoft.2005.12.005.
EnergyPlus DT, 2019. EnergyPlus Development Team. Engineering documentation: EnergyPlus 9.6, The U.S. Department of Energy. Sept. 23, 2021. Accessible at. https://energyplus.net/assets/nrel_custom/pdfs/pdfs_v9.6.0/EngineeringReference.pdf.
Ercolani, G., Chiaradia, E.A., Gandolfi, C., Castelli, F., Masseroni, D., 2018. Evaluating performances of green roofs for stormwater runoff mitigation in a high flood risk urban catchment. J. Hydrol. 566, 830–845. https://doi.org/10.1016/j.jhydrol.2018.09.050.
Faivre, N., Fritz, M., Freitas, T., de Boissezon, B., Vandewoestijne, S., 2017. Nature-based solutions in the EU: innovating with nature to address social, economic and environmental challenges. Environ. Res. 159, 509–518. https://doi.org/10.1016/j.envres.2017.08.032.
Feitosa, R.C., Wilkinson, S., 2016. Modelling green roof stormwater response for different soil depths. Landsc. Urban Plan. 153, 170–179. https://doi.org/10.1016/j.landurbplan.2016.05.007.
Fragkias, M., Lobo, L., Strumsky, D., Seto, K.C., 2013. Does size matter? Scaling of CO2 emissions and US urban areas. PloS One 8 (6), e64727. https://doi.org/10.1371/journal.pone.0064727.
Getter, K.L., Rowe, D.B., Andresen, J.A., 2007. Quantifying the effect of slope on extensive green roof stormwater retention. Ecol. Eng. 31 (4), 225–231. https://doi.org/10.1016/j.ecoleng.2007.06.004.
Getter, K.L., Rowe, D.B., Andresen, J.A., Wichman, S.I., 2011. Seasonal heat flux properties of an extensive green roof in a Midwestern U.S. climate. Energ. Buildings 43, 3548–3557. https://doi.org/10.1016/j.enbuild.2011.09.018.
Guswa, A.J., Celia, M.A., Rodriguez-Iturbe, I., 2002. Models of soil moisture dynamics in ecohydrology: a comparative study. Water Resour. Res. 38 (9), 1166.
Hakimdavar, R., Culligan, P.J., Guido, A., McGillis, W.R., 2016. The Soil Water Apportioning Method (SWAM): an approach for long-term, low-cost monitoring of green roof hydrologic performance. Ecol. Eng. 93 (2016), 207–220. https://doi.org/10.1016/j.ecoleng.2016.05.023.
Hernes, R.R., Gragne, A.S., Abdalla, E.M.H., Braskerud, B.C., Alfredsen, K., Muthanna, T. M., 2020. Assessing the effects of four SUDS scenarios on combined sewer overflows in Oslo, Norway: evaluating the low-impact development module of the Mike Urban model. Hydrol. Res. https://doi.org/10.2166/nh.2020.070.
IPCC, 2021. Climate change 2021: the physical science basis. In: Masson-Delmotte, V., Zhai, P., Pirani, A., et al. (Eds.), Contribution of Working Group I to the Sixth Assessment Report of the Intergovernmental Panel on Climate Change. Cambridge University Press, Cambridge. https://doi.org/10.1017/9781009157896.
Ippolito, M., De Caro, D., Cannarozzo, M., Provenzano, G., Ciraolo, G., 2024. Evaluation of daily crop reference evapotranspiration and sensitivity analysis of FAO Penman-Monteith equation using ERA5-Land reanalysis database in Sicily, Italy. Agricultural Water Management 295, 108732. https://doi.org/10.1016/j.agwat.2024.108732.
Jeffers, S., Garner, B., Hidalgo, D., Daoularis, D., Warmerdam, O., 2022. Insights into green roof modeling using SWMM LID controls for detention-based designs. CHI Journal of Water Management Modeling 30. https://doi.org/10.14796/JWMM.C484.
Jenkins, A., 2020. Biotic systems as a critical urban infrastructure during crisis: learning from the COVID-19 pandemic. Cities & Health 1–3.
Johannessen, B.G., Hamouz, V., Gragne, A.S., Muthanna, T.M., 2019. The transferability of SWMM model parameters between green roofs with similar build-up. J. Hydrol. 569, 816–828. https://doi.org/10.1016/j.jhydrol.2019.01.004.
Lamera, C., Becciu, G., Rulli, M.C., Rosso, R., 2014. Green roofs effects on the urban water cycle components. Procedia Eng. 70, 988–997. https://doi.org/10.1016/j.proeng.2014.02.110.
Lee, J.G., Selvakumar, A., Alvi, K., Riverson, J., Zhen, J.X., Shoemaker, L., Lai, F.H., 2012. A watershed-scale design optimization model for stormwater best management practices. Environ. Model. Software 37, 6–18. https://doi.org/10.1016/j.envsoft.2012.04.011.
Li, Y., Babcock Jr., R.W., 2016. A simplified model for modular green roof hydrologic analyses and design. Water 2016 (8), 343. https://doi.org/10.3390/w8080343.
Liu, W., Feng, Q., Chen, W., Wei, W., Deo, R.C., 2019. The influence of structural factors on stormwater runoff retention of extensive green roofs: new evidence from scale-based models and real experiments. J. Hydrol. 569, 230–238. https://doi.org/10.1016/j.jhydrol.2018.11.066.
Lo Conti, F., Francipane, A., Pumo, D., Noto, L.V., 2015. Exploring single polarization X-band weather radar potentials for local meteorological and hydrological applications. J. Hydrol. 531 (Part 2), 508–522. https://doi.org/10.1016/j.jhydrol.2015.10.071.
Locatelli, L., Mark, O., Mikkelsen, P.S., Arnbjerg-Nielsen, K., Jensen, M.B., Binning, P.J., 2014. Modelling of green roof hydrological performance for urban drainage applications. J. Hydrol. 519 (2014), 3237–3248. https://doi.org/10.1016/j.jhydrol.2014.10.030.
Manfreda, S., Fiorentino, M., Iacobellis, V., 2005. DREAM: a distributed model for runoff, evapotranspiration, and antecedent soil moisture simulation. Adv. Geosci. 2, 31–39. http://www.adv-geosci.net/2/31/2005/.
Noto, L.V., Cipolla, G., Francipane, A., Pumo, D., 2023. Climate change in the Mediterranean basin (part I): induced alterations on climate forcings and hydrological processes. Water Resour. Manag. 37, 2287–2305. https://doi.org/10.1007/s11269-022-03400-0.
Peng, Z., Stovin, V., 2017. Independent validation of the SWMM green roof module. J. Hydrol. 22 (9).
Pörtner, H.O., Scholes, R.J., Arneth, A., Barnes, D.K.A., et al., 2023. Overcoming the coupled climate and biodiversity crises and their societal impacts. Science 380, eabl4881. https://doi.org/10.1126/science.abl4881.
Pumo, D., Viola, F., Noto, L.V., 2008. Ecohydrology in Mediterranean areas: a numerical model to describe growing seasons out of phase with precipitation. Hydrol. Earth Syst. Sci. 12 (1), 303–316. https://doi.org/10.5194/hess-12-303-2008.
Pumo, D., Francipane, A., Alongi, F., Noto, L.V., 2023a. The potential of multilayer green roofs for stormwater management in urban area under semi-arid Mediterranean climate conditions. J. Environ. Manage. 326, 116643. https://doi.org/10.1016/j.jenvman.2022.116643.
Pumo, D., Alongi, F., Cannarozzo, M., Noto, L.V., 2023b. Climate adaptive urban measures in Mediterranean areas: thermal effectiveness of an advanced multilayer green roof installed in Palermo (Italy). Build. Environ. 243, 110731. https://doi.org/10.1016/j.buildenv.2023.110731.
Raymond, C.M., Frantzeskaki, N., Kabisch, N., Berry, P., Breil, M., et al., 2017. A framework for assessing and implementing the co-benefits of nature-based solutions in urban areas. Environ. Sci. Policy 77, 15–24. https://doi.org/10.1016/j.envsci.2017.07.008.
Rodriguez-Iturbe, I., Porporato, A., 2004. Ecohydrology of Water-Controlled Ecosystem: Soil Moisture and Plant Dynamics. Cambridge University Press, Cambridge.
Rossman, L.A., 2015. Storm water management model user's manual version 5.1. EPA/600/R-14/413b, National Risk Management Laboratory Office of Research and Development. United States Environmental Protection Agency, Cincinnati, Ohio., September, 352. http://nepis.epa.gov/Exe/ZyPDF.cgi?Dockey=P100N3J6.TXT.
Santamouris, M., 2020. Recent progress on urban overheating and heat island research. Integrated assessment of the energy, environmental, vulnerability and health impact. Synergies with the global climate change. Energ. Buildings 207, 109482. https://doi.org/10.1016/j.enbuild.2019.109482.
Schrieke, D., Szota, C., Williams, N.S.G., Farrell, C., 2023. Evaluating the effectiveness of spontaneous vegetation for stormwater mitigation on green roofs. Sci. Total Environ. 898, 165643. https://doi.org/10.1016/j.scitotenv.2023.165643.
Seddon, N., Smith, A., Smith, P., Key, I., Chausson, A., et al., 2021. Getting the message right on nature-based solutions to climate change. Glob. Change Biol. 27, 1518–1546. https://doi.org/10.1111/gcb.15513.
Seizarwati, W., Syahidah, M., 2021. Rainfall-runoff simulation for water availability estimation in small island using distributed hydrological model wflow. IOP Conf.

Ser.: Earth Environ. Sci. 930, 012050. https://doi.org/10.1088/1755-1315/930/1/012050.
Shafique, M., Kim, R., Lee, D., 2016. The potential of green-blue roof to manage storm water in urban areas. Nature Environment and Pollution Technology 15 (2), 715–718.
Soulis, K.X., Valiantzas, J.D., Ntoulas, N., Kargas, G., Nektarios, P.A., 2017. Simulation of green roof runoff under different substrate depths and vegetation covers by coupling a simple conceptual and a physically based hydrological model. J. Environ. Manage. 200, 434–445. https://doi.org/10.1016/j.jenvman.2017.06.012.
Spolek, G., 2008. Performance monitoring of three ecoroofs in Portland. Oregon. Urban Ecosyst. 11 (4), 349–359. https://doi.org/10.1007/s11252-008-0061-z.
Stanić, F., Cui, Y.J., Delage, P., de Laure, E., Versini, P.A., et al., 2019. A device for the simultaneous determination of the water retention properties and the hydraulic conductivity function of an unsaturated coarse material; application to a green-roof volcanic substrate. Geotechnical Testing Journal 43 (3), 20170443. https://doi.org/10.1520/GTJ20170443.hal-03045911.
Stanić, F., Delage, P., Cui, Y.J., de Laure, E., 2020. Water retention and transfer properties of a Green roof volcanic substrate. E3S Web of Conferences 195, 03011. https://doi.org/10.1051/e3sconf/202019503011 (E-UNSAT 2020).
Suszanowicz, D., Kolasa Więcek, A., 2019. The impact of green roofs on the parameters of the environment in urban areas—review. Atmosphere 10, 792. https://doi.org/10.3390/atmos10120792.
UN, 2015. United Nations general assembly 2015. Transforming our world: the 2030 agenda for sustainable development, 21 October 2015, A/RES/70/1. Available at: https://www.refworld.org/docid/57b6e3e44.html (Accessed 21 Febrary 2024).
UN, 2019. United Nations, Department of Economic and Social Affairs, Population Division. World Urbanization Prospects: The 2018 Revision (ST/ESA/SER.A/420). United Nations, New York. https://population.un.org/wup/Publications/Files/WUP2018-Report.pdf.
Versini, P.A., Ramier, D., Berthier, E., De Gouvello, B., 2015. Assessment of the hydrological impacts of green roof: from building scale to basin scale. J. Hydrol. 524, 562–575. https://doi.org/10.1016/j.jhydrol.2015.03.020.
Vertessy, R.A., Elsenbeer, H., 1999. Distributed modeling of storm flow generation in an Amazonian rain forest catchment: effects of model parameterization. Water Resour. Res. 35 (7), 2173–2187.
Vijayaraghavan, K., 2016. Green roofs: a critical review on the role of components, benefits, limitations and trends. Renew. Sustain. Energy Rev. 57, 740–752.
Viola, F., Pumo, D., Noto, L.V., 2014. EHSM: a conceptual ecohydrological model for daily streamflow simulation. Hydrol. Process. 28, 3361–3372. https://doi.org/10.1002/hyp.9876.
von Schuckmann, K., Minière, A., Gues, F., et al., 2023. Heat stored in the Earth system 1960–2020: where does the energy go? Earth Syst. Sci. Data. https://doi.org/10.5194/essd-15-1675-2023.
Willmott, C.J., Robeson, S.M., Matsuura, K., 2012. A refined index of model performance. Int. J. Climatol. 32, 2088–2094. https://doi.org/10.1002/joc.2419.
Yan, J., Zhang, F., Zhang, S., Liu, W., et al., 2024. Stormwater retention capacity of blue-green roofs with various configurations: observational data and modelling. Journal of Hydrology 645 (Part A), 132092. https://doi.org/10.1016/j.jhydrol.2024.132092.
Yang, J., Yu, Q., Gong, P., 2008. Quantifying air pollution removal by green roofs in Chicago. Atmos. Environ. 42 (31), 7266–7273. https://doi.org/10.1016/j.atmosenv.2008.07.003.